Empirical Recovery Performance of Fourier-based Deterministic Compressed Sensing

by

Ying Li

A thesis

Presented to Lakehead University

in Partial Fulfillment of the Requirement for the Degree of

Master of Science

in

Electrical and Computer Engineering

Lakehead University

Thunder Bay, Ontario, Canada
May 3rd, 2013

Abstract

Compressed sensing is a novel technique where one can recover sparse signals from the undersampled measurements. Mathematically, measuring an N-dimensional signal $\mathbf{x} \in \mathbb{R}^N$ with a $K \times N$ measurement matrix $\mathbf{\Phi}$ yields a K-dimensional vector $\mathbf{y}$, $\mathbf{y} = \mathbf{\Phi x}$, where $K < N$. In recent years, many researchers demonstrated that a sensing matrix $\mathbf{\Phi}$ plays a vital role in recovery of sparse signals. In terms of the drawbacks of random sensing matrices, deterministic sensing matrices have been sought to apply for the measurement strategies. The deterministic sensing matrices can guarantee the reconstruction performance that is empirically reliable, with fast processing and low complexity.

In this thesis, a Fourier-based deterministic sensing matrix is analyzed and applied for deterministic compressed sensing. Based on the construction of this sensing matrix, we deliberately make experiments to compare the recovery performance of Fourier-based deterministic sensing matrix to that of chirp sensing codes and random partial Fourier sensing matrices in terms of empirical recovery performance in noiseless and noisy scenarios. In image reconstruction, the original image can be sparsified by Haar wavelets and then the largest coefficients of the image have been kept for the image reconstructions. Then, Fourier-based deterministic sensing matrices have been applied to the sparsified image to compare the recovery performance with that of random partial Fourier and chirp sensing matrices. Exploiting the structure of the Fourier-based deterministic sensing matrix, the compressive sampling matching pursuit (CoSaMP) algorithm with an efficient fast Fourier transform (FFT) technique is applied for signal and image reconstruction. Finally, experimental results show that the Fourier-based deterministic sensing matrices, together with the CoSaMP greedy recovery algorithm, can empirically guarantee the sparse signal and image recovery with high reliability.

Acknowledgements

Hereby I would like to express my utmost gratitude to my supervisor Dr. Nam Yul Yu whose sincerity and support I will never forget. Dr. Nam Yul Yu has been my inspiration as I hurdle all the obstacles in the completion this thesis. I would like to thank my family and friends for the love and support during the graduate school, and always. I also would like to thank the other members of my committee, Dr. Ruizhong Wei, Dr. Hassan Naser, for their suggestions and professional guidance.

Ying Li

Table of Contents

Abstract i

Acknowledgements ii

List of Figures iv

List of Tables vi

List of Abbreviations vii

Chapter 1 Introduction 1

1.1 Motivation 2

1.2 Contribution 3

Chapter 2 Background 4

2.1 Compressed Sensing 4

2.2 Noisy Compressed Sensing 7

2.3 Haar Wavelet Transform 7

2.4 Random Partial Fourier Sensing Matrix 8

2.5 Chirp Sensing Codes 10

2.6 RIP and StRIP 11

2.7 Orthogonal Matching Pursuit Algorithm 12

2.8 CoSaMP Algorithm 14

Chapter 3 Fourier-based Deterministic Sensing Matrix 17

3.1 Fourier-based Deterministic Sensing Matrix **A** 17

3.2 Statistical Restricted Isometry Property for **A** 21

3.3 FFT-based Signal Measurement and Recovery 22

3.3.1 Measurement 22

3.3.2 Reconstruction 23

Chapter 4 Empirical Experiments 26

4.1 Comparison between OMP and CoSaMP 27
4.2 Recovery Performance for Compressed Sensing 29
4.2.1 Successful Recovery Rate with Noiseless Signals 31
4.2.2 Reconstruction SNR with Noiseless Signals 36
4.3 Recovery Performance for Noisy Compressed Sensing 41
4.3.1 Reconstruction SNR with Noisy Signals 41
4.3.2 Reconstruction SNR vs. Input SNR 46
4.4 Image Reconstruction 51
Chapter 5 Conclusions 55

List of Figures

2.1 The process of the traditional data acquisition……..…….……4

2.2 Compressed sensing based datat acqusition……..……5

3.1 Concatenated structure of Fourier-besed deterministic sensing matrix **A**…….....18

3.2 The signal measurement with FFT algorithm…….…..23

3.3 The signal reconstruction with FFT algorithm……..25

4.1 The comparison between CoSaMP and OMP in successful recovery rate when $L = 4$……..……...…….28

4.2 The comparison between CoSaMP and OMP in successful recovery rate when $L = 8$……..……....…….29

4.3 Successful recovery rates of the Fourier-based deterministic, random partial Fourier and chirp sensing matrices for $L = 4$ from noiseless measurement……32

4.3 Successful recovery rates of the Fourier-based deterministic, random partial Fourier and chirp sensing matrices for $L = 4$ from noiseless measurement……33

4.4 Successful recovery rates of the Fourier-based deterministic, random partial Fourier and chirp sensing matrices for $L = 8$ from noiseless measurement……34

4.4 Successful recovery rates of the Fourier-based deterministic random partial Fourier and chirp sensing matrices for $L = 8$ from noiseless measurement……35

4.5 Reconstruction SNR of the Fourier-based deterministic, random partial Fourier and chirp sensing matrices for $L = 4$ from noiseless measurement……...…37

4.5 Reconstruction SNR of the Fourier-based deterministic, random partial Fourier and chirp sensing matrices for $L = 4$ from noiseless measurement……..38

4.6 Reconstruction SNR of the Fourier-based deterministic, random partial Fourier and chirp sensing matrices for $L = 8$ from noiseless measurement……40

4.6 Reconstruction SNR of the Fourier-based deterministic, random partial Fourier and chirp sensing matrices for $L = 8$ from noiseless measurement…….....40

4.7 Reconstruction SNR of the Fourier-based deterministic, random partial Fourier and chirp sensing matrices in noisy compressed sensing for $L = 4$ with $\mathrm{SNR}_{\mathrm{input}} = 15$ dB……42

4.7 Reconstruction SNR of the Fourier-based deterministic, random partial Fourier and chirp

sensing matrices in noisy compressed sensing for $L = 4$ with $\mathrm{SNR}_{\mathrm{input}} = 15$ dB……..43

4.8 Reconstruction SNR of the Fourier-based deterministic, random partial Fourier and chirp sensing matrices in noisy compressed sensing for $L = 8$ with $\mathrm{SNR}_{\mathrm{input}} = 15$ dB…….....44

4.8 Reconstruction SNR of the Fourier-based deterministic, random partial Fourier and chirp sensing matrices in noisy compressed sensing for $L = 8$ with $\mathrm{SNR}_{\mathrm{input}} = 15$ dB…….....45

4.9 Reconstruction SNR vs. Input SNR in noisy scenario of 25-sparse input signal when $L = 4$……...…….....47

4.9 Reconstruction SNR vs. Input SNR in noisy scenario of 40-sparse input signal when $L = 4$…….....48

4.10 Reconstruction SNR vs. Input SNR in noisy scenario of 33-sparse when $L = 8$…….....49

4.10 Reconstruction SNR vs. Input SNR in noisy scenario of 70-sparse when $L = 8$…….....50

4.11 The process of image sparsification with Haar wavelet……..……51

4.12 Original image, wavelet coefficients and sparsified image …….....52

4.13 The comparison in recovery performance of 7% sparsified Cameraman…….....54

List of Tables

2.1 OMP recovery algorithm……..……13

2.2 CoSaMP recovery algorithm……..15

4.1 Various parameters of $K = p^r$ in the experiments……..25

4.2 The comparison in reconstruction SNR of 7% sparsified Cameraman…….....53

List of Abbreviations

Abbreviation	Meaning
DFT	Discrete Fourier transform
IDFT	Inverse discrete Fourier transform
FFT	Fast Fourier transform
CoSaMP	Compressive sampling matching pursuit
OMP	Orthogonal matching pursuit
RIP	Restricted isometry property
StRIP	Statistical restricted isometry property
SNR	Signal-to-noise ratio

Chapter 1

Introduction

Compressed sensing (or compressive sampling) as a novel and emerging technology has been proposed by Donoho [1], Candes and Tao [2] [3], which provides a fundamentally new approach for sampling signals. Compared to the traditional *Nyquist* sampling theorem, compressed sensing predicts that certain signals or images can be recovered if they are sparse or compressible with respect to some basis or dictionary of waveforms [4].

In recent years, many researchers demonstrated that a measurement matrix **A** plays a vital role in recovery of sparse signals. Random sensing matrices, such as Gaussian and Bernoulli random matrices have been investigated for a long time with so many theoretical benefits [5], but the drawbacks [6] of high complexity, large storage, and low efficiency are obvious as well in its practical implementation. Considering the drawbacks, a few research activities have sought to develop a deterministic matrix to apply for the measurement strategies, e.g. chirp sequences [7], Kerdock and Delsarte-Goethals codes [8, 9] , dual BCH codes [10] and second order Reed-Muller codes [11]. Other techniques for deterministic construction, based on finite fields, representation theory, and character sequences, can be found in [12-17]. The deterministic matrices can guarantee the reconstruction performance that is empirically reliable, with fast processing and low complexity.

1.1 Motivation

Recently, Yu, Feng, Zhang present a new class of near-optimal (N, K) partial Fourier codebooks in [12]. They demonstrate that by arranging each code vector as a column, the new near-optimal codebook presents a $K \times N$ partial Fourier matrix with near-optimal coherence and tightness by choosing the rows deterministically from the inverse discrete Fourier transform (IDFT) matrix.

Inspired by the theoretical construction of a Fourier-based deterministic sensing matrix in [18] and motivated by the experiments in [19], we compare recovery performances of the Fourier-based deterministic sensing matrices to those of random partial Fourier and chirp sensing matrices in the noiseless, noisy scenarios and image reconstruction, respectively. Note that the idea behind this work is that we expect this Fourier-based deterministic sensing matrix to inherit the numerical reliability and low complexity in the practical implementation, and also to provide more options with various applications.

1.2 Contribution

In this thesis, we first deliberately make experiments to compare the recovery performance of compressive sampling matching pursuit (CoSaMP) [21] and orthogonal matching pursuit (OMP) [44] reconstruction algorithms. Moreover, the Fourier-based deterministic sensing matrix has been compared to chirp sensing codes [7] and random partial Fourier sensing matrices in terms of empirical recovery performance with noiseless and noisy scenarios. The original image can be computed by Haar wavelets [32] and then the largest coefficients of the image have been kept for the image reconstructions. Then, Fourier-based deterministic sensing matrix is applied to the sparsified image to compare the recovery performance with that of random partial Fourier and chirp sensing matrix. Finally, experimental results show that the Fourier-based deterministic sensing matrices, together with the CoSaMP greedy algorithm, can empirically guarantee the sparse signal and image recovery with high reliability.

The contributions of analysis and applications of Fourier-based deterministic sensing matrix can be summarized as follows.

- We make experiments to compare recovery performance of CoSaMP and OMP with the Fourier-based deterministic sensing matrix.
- Numerical experiments demonstrate reliable reconstruction performance with CoSaMP recovery algorithm in noiseless and noisy scenarios, respectively.
- Haar wavelet transform is applied to sparsify the original image
- The Fourier-based deterministic sensing matrix is applied to image reconstruction.
- The performance of Fourier-based deterministic sensing matrix is compared to random partial Fourier sensing matrix and chirp sensing code in image reconstruction.

Chapter 2

Background

2.1 Compressed Sensing

The traditional method to reconstruct images or signals from measured data follows the *Shannon/Nyquist* sampling theorem. It states that if the samples of a signal are taken at *Nyquist rate* or twice the highest frequency, which can be perfectly reconstructed from its measurements. This principle underlies most devices of current technology, such as analog to digital conversion, medical imaging or audio and video electronics [22]. However, in many important applications, *Nyquist rate* is so high by ending up with far too many samples. Due to the cost and physical limitation, the data acquisition and processing of signals in application areas such as imaging, video, medical imaging continues to be concerned. The process of traditional data acquisition is shown below.

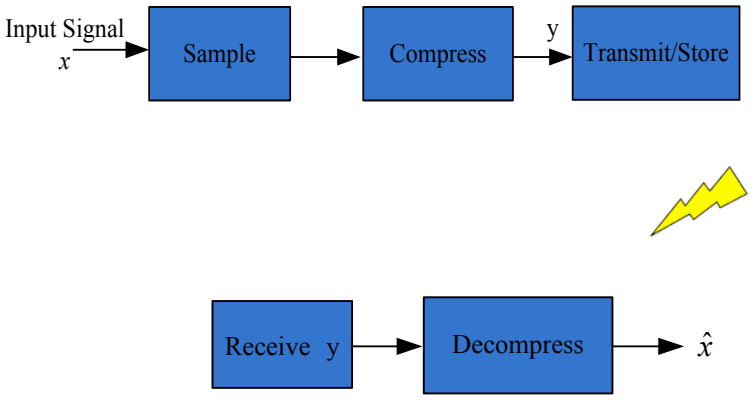

Figure 2.1 The process of the traditional data acquisition

To address these challenges to deal with the high-dimensional data, we turn our attention to compression, the purpose of which is to obtain the most succinct

representation of the original signal and to achieve the acceptable distortion in data. Transform coding, one of the most popular techniques for signal compression, typically dedicates on finding a basis or frame that provides sparse or compressible representations for signals [23]. Sparse representation, in particular, is a common way to sparsify a signal by transforming the signal to the orthonormal basis (E.g. Wavelet basis [32]). Both sparse and compressible signals can be represented with high fidelity by preserving only the values and locations of the largest coefficients of the signal. For example, the commercial coding standards MP3 [25], JPEG [26], and JPEG2000 [27] can directly exploit this sparsity.

However, because typical signals have some structure, the process of massive data acquisition followed by compression is extremely wasteful. Compressed sensing [1], as an emerging and novel technology indicates that when the signal is sparse or compressible, the signal can be recovered accurately or approximately from the incomplete measurements, which accomplishes the combination of sampling and compression. Figure 2.2 is presenting the compressed sensing based data acquisition system.

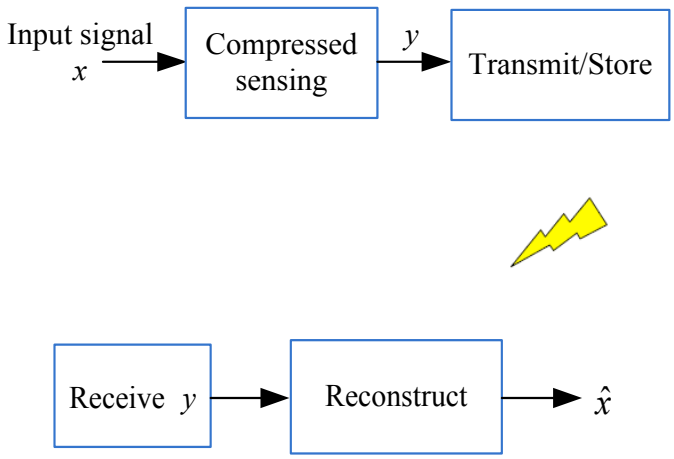

Figure 2.2 Compressed sensing based data acquisition system

In practice, particularly the medical imaging applications such as Magnetic Resonance Imaging (MRI) [28], computed tomography (CT) [29] and ultrasound can be very well suited to compressed sensing. Specifically, we use MRI as an example to

illustrate that how compressed sensing works in medical application. MRI obeys two key requirements for successful application of compressed sensing: (1) medical imagery is naturally compressible by sparse coding in an appropriate transform domain (e.g., by wavelet transform); (2) MRI scanners naturally acquire samples of the encoded image in spatial frequency, rather than direct pixel samples [28].

Mathematically, measuring an N-dimensional signal $\mathbf{x} \in \mathbb{R}^N$ with a $K \times N$ measurement matrix $\mathbf{\Phi}$ yields a K-dimensional vector $\mathbf{y}$, $\mathbf{y} = \mathbf{\Phi x}$, where $K < N$. We assume that $\mathbf{x}$ can be sparsified in some orthonormal basis $\mathbf{\Psi}$. Thus, we can write $\mathbf{x}$ as in [30]

$$\mathbf{x} = \mathbf{\Psi s} \tag{2.1}$$

where $\mathbf{s}$ is a length $N \times 1$ column vector. We measure $\mathbf{x}$ with $K < N$ projections which have results given in the vector $\mathbf{y}$. The vectors projected upon are set as the rows of the $K \times N$ matrix $\mathbf{\Phi}$ which gives in [30]

$$\mathbf{y} = \mathbf{\Phi \Psi s}$$

$$= \mathbf{\Theta s} \tag{2.2}$$

where $\mathbf{\Theta} = \mathbf{\Phi \Psi}$ is a $K \times N$ matrix. We are free to design $\mathbf{\Psi}$ and thus $\mathbf{\Theta}$. Though, if we design $\mathbf{\Theta}$ we should remain aware that actual sensing of the signal is done with the orthonormal basis $\mathbf{\Psi}$.

The main considerations from (2.1) and (2.2) can be highlighted as follows:

1) For signal $\mathbf{x} \in \mathbb{R}^N$, we need to find the orthogonal basis $\mathbf{\Psi}$, then sparse representation of $\mathbf{x}$ can be performed on $\mathbf{\Psi}$.
2) We need to design a measurement matrix which is uncorrelated with $\mathbf{\Psi}$ [2].
3) A reconstruction algorithm should be designed for recovering accurately the original input signal $\mathbf{x}$.

2.2 Noisy Compressed Sensing

Now, we turn our attention to noisy compressed sensing. Sparse signal recovery in the presence of noise has been intensively investigated in many recent literatures because real-world devices are subject to at least a small amount of noise [31]. The noisy measurement is represented as

$$\mathbf{u} = \mathbf{y} + \mathbf{z} = \mathbf{\Phi x} + \mathbf{z} \tag{2.3}$$

where the measurements are corrupted by $\mathbf{z}$, which is the additive white Gaussian noise of zero mean and variance σ^2.

2.3 Haar Wavelet Transform

For image processing, most coefficients of an image are very small, and only the relatively few large coefficients contain most of the important information. Wavelet transfrom [32] is similar to Fourier transform in that it allows a target function over an interval to be represented in terms of an orthogonal function basis [32].

The Haar transform is one of the simplest and basic transformations from the space/time domain to a local frequency domain, which reveals the space/time-variant spectrum. Attracting feature of Haar transform is that it can analyze the local features. This property makes it applicable in electrical and computer engineering applications, such as signal and image compression. The Haar sequence is now recognized as the first known and the simplest wavelet basis [33].

Mathematically, we have a vector $\mathbf{f} \in \mathbb{R}^n$ in which we use a Haar wavelet transform basis $\mathbf{\Psi} = [\,\Psi_1\ \Psi_2 \ldots \Psi_n]$ as follows in [34]:

$$\mathbf{f}(\mathrm{t}) = \sum_{i=1}^{n} x_i \Psi_i(\mathrm{t}) \tag{2.4}$$

where $1 \leq i \leq n$, x is the coefficient sequence of $\mathbf{f}$, $x_i = <\mathbf{f}, \Psi_i>$.

Example 1. The 4×4 Haar wavelet transform matrix shown below:

$$\mathcal{H} = \frac{1}{\sqrt{4}}\begin{bmatrix} 1 & 1 & 1 & 1 \\ 1 & 1 & -1 & -1 \\ \sqrt{2} & -\sqrt{2} & 0 & 0 \\ 0 & 0 & \sqrt{2} & -\sqrt{2} \end{bmatrix}$$

In image reconstruction part of our experiments, we apply the Haar wavelet transform matrix to an original image signal, where one can discard small coefficients without losing the significant information. Formally, consider $\mathbf{f}_{\boldsymbol{s}}(\mathrm{t})$ obtained by keeping only the terms corresponding to the s largest values in the sparsity representation.

2.4 Random Partial Fourier Sensing Matrix

First, let us discuss that a DFT matrix is an expression of a discrete Fourier transform (DFT) as a matrix multiplication. By collecting the DFT output samples into a column vector as follows.

$$\underbrace{\begin{bmatrix} X(w_0) \\ X(w_1) \\ X(w_2) \\ . \\ . \\ . \\ X(w_{N-1}) \end{bmatrix}}_{\boldsymbol{X}} = \underbrace{\begin{bmatrix} A_0(0) & A_0(1) & \dots & A_0(N-1) \\ A_1(0) & A_1(1) & \dots & A_1(N-1) \\ A_2(0) & A_2(1) & \dots & A_2(N-1) \\ & & . & \\ & & . & \\ & & . & \\ A_{N-1}(0) & A_{N-1}(1) & \dots & A_{N-1}(N-1) \end{bmatrix}}_{\mathbf{A}'_N} \underbrace{\begin{bmatrix} x(0) \\ x(1) \\ x(2) \\ . \\ . \\ . \\ x(N-1) \end{bmatrix}}_{\mathbf{x}}$$

where $\mathbf{x}$ is the input signal. Therefore, the inverse DFT operation can be performed as

$$\mathbf{x} = \frac{1}{N}\mathbf{A}_N \cdot \boldsymbol{X} \tag{2.5}$$

where $\mathbf{A}_N$ is the N-point IDFT matrix. The nth column of $\mathbf{A}_N$ is denoted as $\mathbf{a}_n$ and the kth row of $\mathbf{a}_n$, denoted as $\mathbf{A}_n(k)$, is $e^{\frac{2\pi jkn}{N}}$.

Mathematically, the N-point inverse discrete Fourier transform (IDFT) of a discrete signal $\boldsymbol{X}(n)$ is defined as in [36]

$$\mathbf{x}(k) = \sum_{n=0}^{N-1} e^{\frac{2\pi jkn}{N}} \boldsymbol{X}(n), \qquad k = 0,1,\dots,N-1 \tag{2.6}$$

where $j = \sqrt{-1}$.

Let $D = \{d_0, \dots d_{K-1}\}$ as defined in [12] be the row index set of selecting K distinct integers, where $0 \le d_k \le N-1$. A $K \times N$ partial Fourier matrix selects K rows from the N-point IDFT matrix. With a scaling factor of $\frac{1}{\sqrt{K}}$, the lth column vector of the partial Fourier matrix is given as

$$\mathbf{A}_{\boldsymbol{l}} = \frac{1}{\sqrt{K}} (e^{j\frac{2\pi d_0 l}{N}}, e^{j\frac{2\pi d_1 l}{N}}, \dots, e^{j\frac{2\pi d_{K-1} l}{N}})^T \quad , 0 \le l \le N-1 \tag{2.7}$$

Then $\mathbf{A} = (\mathbf{A_0}, \mathbf{A_1}, \dots, \mathbf{A}_{N-1})$ is constructed partial Fourier codebook. The coherence [39] of $\mathbf{A}$ is given by

$$\mu = \max_{0 \le n_1 \ne n_2 \le N-1} \left| \mathbf{a}_{n_1}^H \mathbf{a}_{n_2} \right| = \frac{1}{\sqrt{K}} \tag{2.8}$$

where $\mathbf{a}_{n_1}$ is a column vector of $\mathbf{A}$ and $\mathbf{a}_{n_1}^H$ denotes its complex conjugate. The coherence can almost achieve the Welch bound equality [40] and sufficiently large N. Moreover, $\mathbf{A}$ forms tightness [41] as each row is mutually orthogonal.

Finally, a random partial Fourier matrix is constructed by choosing K rows uniformly at random from the $N \times N$ inverse DFT matrix, equivalent to the partial Fourier codebook proposed in [12] and [38]. In [38], they presented the codebook for $p = 2$ from the array structure of binary m-sequences and their Fourier transforms. It was then generalized for any prime p in [12], where its proof was also improved by utilizing a new almost difference set.

2.5 Chirp Sensing Codes

Chirp sensing code as a deterministic sensing matrix has been proposed and presented by Applebaum et al. [7], which is designed with chirp signals forming the columns. Specifically, an n-length *chirp* signal with *chirp* rate r and base frequency m is given as

$$\phi_{r,m}(\ell) = \frac{1}{\sqrt{n}} e^{\frac{2\pi j}{n} r\ell^2 + \frac{2\pi j}{n} m\ell}, \qquad r, m, \ell \in \mathbb{Z}_n \tag{2.9}$$

where $\frac{1}{\sqrt{n}}$ is the coefficient to guarantee the vector to have the unit form, ℓ represents row index of $\mathbf{\Phi}_{chirp}$. For a chirp signal with n length, there are n^2 possible pairs (r, m). Therefore, it is clear to have the full size of chirp sensing codes with $n \times n^2$ as follows

$$\mathbf{\Phi}_{chirp} = [\mathbf{V}_1, \mathbf{V}_2, \dots\dots, \mathbf{V}_n] \tag{2.10}$$

Each $n \times n$ submatrix $\mathbf{V}_i$, where $1 \le i \le n$, with columns given by chirp signals having a fixed chirp rate r_i, with m runs through 0 to $n-1$, the chirp rate r also varies from 0 to $n-1$. Therefore, column $j = m + rn + 1$ of $\mathbf{\Phi}_{chirp}$ is a discrete chirp with chirp rate r and base frequency m.

In [7], they compared the statistics of eigenvalues of the Grammitain matrices to those of n columns chosen uniformly at random from the chirp matrix. Also, $\mathbf{\Phi}_{chirp}$ can satisfy the UStRIP property in [6] that it can be suitable as compressed sensing measurement in general.

As explained in [19, 43], because of the sparsity of signals or images and the rule of thumb, not only the full size of $\mathbf{\Phi}_{chirp}$ can be used as the sensing matrix, but a few sub-matrices can do as well. In practice, the compression ratio n/N is more free to use for the sparse signals or images.

Example 2. The submatrix of chirp sensing codes can be

$$\mathbf{\Phi}_{chirp} = \left[\mathbf{V}_{r_1}, \mathbf{V}_{r_2}, \mathbf{V}_{r_3}, \widehat{\mathbf{V}}_{r_4}\right] \tag{2.11}$$

where $r_1 = 1$, $r_2 = 2$, $r_3 = 3$, $r_4 = 4$, and $\widehat{\mathbf{V}}_{r_4}$ is a submatrix of $\mathbf{V}_{r_4}$, so that the column number of $\mathbf{\Phi}_{chirp}$ can match the signal size. For instance, the sensing matrix for an 128×128 $(N = 16384)$ image might be taken to be of size $(n, N) = (4093, 16372)$. Note that $n = 4093$ is the closet prime number to 25% of 16384.

However, the limitations of chirp sensing codes is obvious: 1) the restriction must be $n \geq \sqrt{N}$. As a result, this limits the algorithm's abilities in situation where n must be small. 2) n has to be a prime number to uniquely determine r_j[7].

2.6 RIP and StRIP

The restricted isometry property (RIP) [35] of a compressed sensing matrix is an important necessary condition to guarantee the sparse signal recovery.

Theorem 1. *[35] Let* $\mathbf{\Phi}$ *be a* $K \times N$ *matrix. Then* $\mathbf{\Phi}$ *has the Restricted Isometry Property (RIP) of order* s*, if there exists a* $\delta_s \in (0, 1)$ *such that*

$$(1 - \delta_s)||\mathbf{x}||^2 \leq ||\mathbf{\Phi x}||^2 \leq (1 + \delta_s)||\mathbf{x}||^2 \tag{2.12}$$

holds for all s*-sparse vectors* $\mathbf{x}$.

A sensing matrix $\mathbf{\Phi}$ satisfies the restricted isometry property (RIP) if δ_s is not too close to one [35]. The RIP is a very restrictive condition and the currently known measurement matrices obeying the RIP with near-optimal number of measurements drive into two categories [36]: 1) Random matrices such as Gaussian or Bernoulli matrices with the entries of Gaussian or Bernoulli distribution, 2) Random partial Fourier matrix or Hadamard transform matrix are obtained by choosing K rows uniformly at random from a normalized $N \times N$ Fourier or Hadamard transform matrices.

Due to the storage limitations of random matrices, in some applications, deterministic sensing matrices have been put into much desire. Calderbank et al. [6] demonstrated an approach on deterministic sensing matrix on $\boldsymbol{\Phi}$ to ensure that $\boldsymbol{\Phi}$ as a nearly-isometry with high probability regarding to the s-sparse signals on a uniform distribution.

Definition 1. *[6] A* $K \times N$ *matrix* $\boldsymbol{\Phi}$ *is said to be* η*-StRIP-able, where* $0 < \eta \leq 1$*, if the following three conditions are satisfied*

- *The rows of* $\boldsymbol{\Phi}$ *are mutually orthogonal, and all the row sums are equal to zero.*
- *The columns of* $\boldsymbol{\Phi}$ *form a group under pointwise multiplication from which the entries of first column of* $\boldsymbol{\Phi}$ *are set to be constant.*
- *For any* $n \in \{2, \dots, N\}$*,*

$$\left|\sum_{k} \varphi_n(k)\right|^2 \leq K^{1-\eta} \tag{2.13}$$

Remark 1[6]. The third condition is a bound for the absolute value of the column sum of the matrix. For example, we assume that a basic partial Fourier matrix $\boldsymbol{\Phi}$ has the first column of $(\frac{1}{\sqrt{K}}, \frac{1}{\sqrt{K}}, \dots, \frac{1}{\sqrt{K}})^T$, denoted as φ_1, one can check that

$$\left|\sum_{k} \varphi_n(k)\right| = \left|\sqrt{K}{\varphi_1}^H \varphi_n\right|.$$

Thus, the column sum is actually close related to the coherence of this basic partial Fourier matrix.

2.7 Orthogonal Matching Pursuit Algorithm

This section describes an iterative greedy algorithm for signal recovery, known as orthogonal matching pursuit (OMP) algorithm proposed in [44]. This algorithm is a commonly used algorithm for recovery of sparse signals due to its low complexity

and simple implementation.

The procedure of OMP is defined in [44] as follows.

Input:

− A $K \times N$ measurement matrix $\mathbf{A}$

− A K-dimensional measurement vector $\mathbf{y}$

− The sparsity level s

Output:

− An index set Λ containing s elements

− A signal estimate $\hat{\mathbf{x}} \in \mathbb{R}^N$

Table 2.1 OMP Recovery Algorithm [44]

Procedure (OMP):
0) Initialize a residual vector $\mathbf{r_0} = \mathbf{y} = (y_0, \cdots, y_{k-1})^T$ and $\Lambda = \phi$ at iteration $i = 0$.
1) At iteration i, compute $\mathbf{f} = \mathbf{A^H r_i} = (\mathrm{f}_0, \cdots, \mathrm{f}_{N-1})^T$, find the peak of $\mathbf{f}$, and record its position as n_i i.e., $\mathrm{n}_i = \mathrm{argmax}_{t=0,\cdots,N-1}\lvert f\mathrm{t}\rvert$.
2) Update the index set $\Lambda \leftarrow \Lambda \cup \{n_i\}$ and the submatrix $\mathbf{A_{i+1}} = [\mathbf{A_i}\ \mathbf{a_{ni}}]$. Note that $\mathbf{A_0}$ is an empty matrix.
3) Solve a least-square problem to obtain $\boldsymbol{b_i} = \mathrm{argmin}_b \lvert\lvert \mathbf{y} - \mathbf{A_{i+1}b} \rvert\rvert_2$.
4) Update the residual by $\mathbf{r}_{i+1} = \mathbf{y} - \mathbf{A}_{i+1}\,\mathbf{b}_i$.
5) If $i < s-1$, then $i \leftarrow i+1$ and repeat 1) − 4). If $i = s-1$, stop the iteration. The nonzero entry of $\hat{\mathbf{x}}$ is set by $\hat{\mathbf{x}}_{n_j} = \mathbf{b}_j$ for $\mathrm{n}_j \in \Lambda$, where $\mathbf{b}_j$ is the jth element of $\mathbf{b}_{s-1}$.

Note that the measurement procedure in the compressed sensing, i.e., $\mathbf{Ax}$ is a linear combination of s columns in $\mathbf{A}$. In the reconstruction part, we have to

determine which columns of $\mathbf{A}$ participated in this measurement and the coefficients of these columns contributed in the measurement. The idea behind this algorithm is to choose columns in a greedy fashion [43]. At each iteration, we choose the column of $\mathbf{A}$ that is the most strongly correlated with the remaining part of vector $\mathbf{y}$. Then the coefficients of the chosen columns are calculated in a least-square manner. Finally, we subtract off these columns' contribution to $\mathbf{y}$ and iterate on the residual. After s iterations, the algorithm will have identified the correct set of columns together with their corresponding coefficients.

2.8 CoSaMP Algorithm

This section introduces the Compressive Sampling Matching Pursuit (CoSaMP) algorithm described in [21]. The algorithm is useful and general for recovery of sparse signal or image, which will be used in the compressed sensing empirical experiments in Chapter 4.

As input, the CoSaMP algorithm requires four pieces of information:

1) A $K \times N$ measurement matrix $\mathbf{A}$

2) A K-dimensional measurement vector $\mathbf{y}$

3) The sparsity level s of the approximation to be produced.

4) A halting criterion.

The algorithm is initialized with a trivial signal approximation, which means that the initial residual equals the unknown target signal. During each iteration, CoSaMP performs five major steps [21]:

- Identification. The algorithm forms a proxy of the residual from the current samples and locates the largest components of the proxy.
- Support Merger. The new support set is united with the set of components that appear in the current approximation.
- Estimation. The algorithm solves a least-squares problem to approximate the

target signal on the merged set of components.

- Pruning. The algorithm produces a new approximation by retaining only the largest entries in this least-squares signal approximation.
- Sample Update. The samples are updated so that they reflect the residual, the part of the signal that has not been approximated.

These steps are repeated until the hating criterion is triggered. In our experiments, the halting criterion is if the norm of updated samples is very small, e.g.$\left|\left|\mathbf{v}\right|\right| < 10^{-4}$, or the iteration counter $\mathbf{t}$ reaches the sparsity level.

The main procedure of CoSaMP summarizes in Table 2.2

Table 2.2 CoSaMP Recovery Algorithm [21]

$\hat{\mathbf{x}}_0 \leftarrow \mathbf{0}$	
$\mathbf{v} \leftarrow \mathbf{y}$	
$\mathbf{t} \leftarrow \mathbf{0}$	*Iteration*
$\mathbf{b} \leftarrow \mathbf{0}$	*{Current samples=input samples}*
Repeat	
$\boldsymbol{t} \leftarrow \boldsymbol{t} + \mathbf{1}$	
$\mathbf{f} \leftarrow \mathbf{A}^{\boldsymbol{H}}\mathbf{v}$	*Form a signal proxy*
$\boldsymbol{\Omega} \leftarrow \mathbf{supp}(\mathbf{f}_{\mathbf{2s}})$	*Identify large components*
$\mathbf{T} \leftarrow \boldsymbol{\Omega} \cup \mathbf{supp}(\hat{\mathbf{x}}_{\boldsymbol{t-1}})$	*Merge supports*
$\mathbf{b}\vert_{\mathbf{T}} \leftarrow \mathbf{A}_{\mathbf{T}}^{\dagger}\mathbf{y}$	*Estimate signal by least-squares*
$\hat{\mathbf{x}}_{\boldsymbol{t}} \leftarrow \mathbf{b}_{\boldsymbol{s}}$	*Take the largest* $\boldsymbol{s}$ *entries*
$\mathbf{v} \leftarrow \mathbf{y} - \mathbf{A}\hat{\mathbf{x}}_{\boldsymbol{t}}$	*Update current samples*
Until a halting criterion is true	

This algorithm is to approximate the target signal $\hat{\mathbf{x}}$. At the first step, it forms a signal proxy $\mathbf{f}$ and identifies a potential candidate omega of the signal support by

detecting the location of the largest $2s$ components of the proxy. Then it merges the support to generate a new support set $\mathbf{T}$. We use the samples to estimate the target signal $\hat{\mathbf{x}}$ on this support, and take only the largest s entries from the signal approximation $\mathbf{b}$. Finally, it updates current samples $\mathbf{v}$ for next iteration.

In our experiments, the matrix-vector multiplication of $\mathbf{A}\hat{\mathbf{x}}_t$ is performed by the FFT algorithm since the Fourier-based deterministic sensing matrix $\mathbf{A}$ is based on DFT matrix structure, meanwhile current samples are updated at each iteration.

Chapter 3

Fourier-based Deterministic Sensing Matrix

3.1 Fourier-based Deterministic Sensing Matrix A

A basic $p^r \times (p^{2r}-1)$ matrix $\widehat{\mathbf{A}}$ [12] is constructed by choosing p^r rows deterministically from $(p^{2r}-1)$-point inverse discrete Fourier transform (IDFT), where p is a prime number and r is a positive integer. It was then generalized for any prime p in [12].

In this section, based on the basic partial Fourier sensing matrix, a Fourier-based sensing matrix has been studied in [18]. According to the theoretical construction, we analyze and apply the Fourier-based sensing matrix to our empirical experiments in Chapter 4.

Now, we present a formal expression of the construction of Fourier-based deterministic sensing matrix **A**

Construction 1[18]: *Let* $K = p^r$ *be with a prime* p *and a positive integer* r. *Let* $D = \{d_0, \cdots, d_{K-1}\}$ *be the row index set of two cases:* $p = 2$, *or* $p > 2$. *Let* L *be a positive integer and* $N = (K+1)L$, *where* $1 < L \leq K-1$. *For a given integer* l, $0 \leq l \leq L-1$, *define a* $K \times (K+1)$ *submatrix* $\sigma^{(l)} = \{\sigma_{k,t}^{(l)} \mid 0 \leq k \leq K-1, 0 \leq t \leq K\}$ *where if* $p = 2$,

$$\sigma_{k,t}^{(l)} = \frac{1}{\sqrt{K}} exp\left(-j\frac{2\pi(k+1)t}{K+1}\right) \cdot \gamma_k^{(l)} \tag{3.1}$$

or if $p > 2$

$$\sigma_{k,t}^{(l)} = \begin{cases} \frac{1}{\sqrt{K}} exp\left(-j\frac{2\pi(k+1)t}{K+1}\right) \cdot \gamma_{k+\frac{K+1}{2}}^{(l)}, & 0 \le k \le \frac{K-1}{2} \\ \frac{1}{\sqrt{K}} exp\left(-j\frac{2\pi(k+1)t}{K+1}\right) \cdot \gamma_{k-\frac{K-1}{2}}^{(l)}, & \frac{K-1}{2} \le k \le K-1 \end{cases} \quad (3.2)$$

In (3.1) and (3.2), and the constant mask vector $\gamma_\kappa^{(l)}[20]$ is applied to the kth row as $\gamma_\kappa^{(l)} = exp\left(j\frac{\pi d_\kappa l}{K-1}\right) \cdot exp\left(-j\frac{\pi d_\kappa l}{K+1}\right)$. A $K \times N$ sensing matrix $\mathbf{A}$ is constructed by concatenating the L submatrices by varying l, i.e., $\mathbf{A} = (\boldsymbol{\sigma}^{(0)}|\,\boldsymbol{\sigma}^{(1)}|\,\cdots\,|\,\boldsymbol{\sigma}^{(L-1)})$. Particularly, if $L = K + 1$, then $\mathbf{A} = \mathbf{A}' = (\boldsymbol{\sigma}^{(0)}|\,\boldsymbol{\sigma}^{(1)}|\,\cdots\,|\,\boldsymbol{\sigma}^{(K-2)})$.

Figure 3.1 below illustrates the structure of the Fourier-based deterministic sensing matrix $\mathbf{A}$ with $p = 2$ in ***Construction 1***. For $p > 2$, changing the order of row indices yields a similar structure.

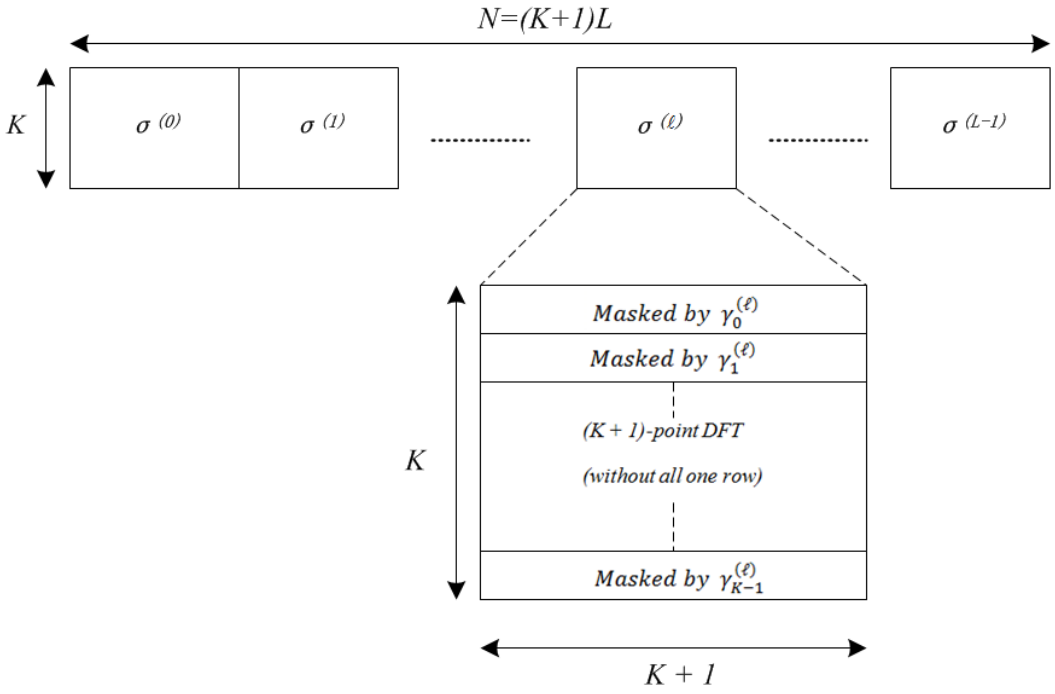

Figure 3.1 Concatenated structure of Fourier-based deterministic sensing matrix $\mathbf{A}$ $(\boldsymbol{p = 2})$

Remark 2: Choosing K rows according to the index set D, then a $K \times N$ basic matrix $\widehat{\mathbf{A}}$ has been constructed in [12], where each entry is given by

$$\hat{a}_{k,n} = \frac{1}{\sqrt{K}} exp\left(j\frac{2\pi d_k n}{N}\right), \quad j = \sqrt{-1} \tag{3.3}$$

for $0 \le k \le K-1$ and $0 \le n \le N-1$

Let l be given for $0 \le l \le K-2$. From $\widehat{\mathbf{A}}$ if we take $K+1$ column vectors of indices $n = (K-1)t + l$ with varying t, where $0 \le t \le K$, the entries of the colum vectors are given by

$$\frac{1}{\sqrt{K}} exp\left(j\frac{2\pi d_\kappa\big((K-1)t+l\big)}{N}\right) = \frac{1}{\sqrt{K}} exp\left(j\frac{2\pi d_\kappa}{K+1}\right) \cdot exp\left(j\frac{2\pi d_\kappa l}{N}\right) \tag{3.4}$$

for $0 \le k \le K-1$. For given l, we define a constant mask factor $\gamma_\kappa^{(l)}$ applied to the kth row in (3.4) as

$$\begin{aligned} \gamma_\kappa^{(l)} &\triangleq exp\left(j\frac{2\pi d_\kappa l}{N}\right) \\ &\triangleq exp\left(j2\pi d_\kappa l \cdot \frac{1}{2}\left(\frac{1}{K-1} - \frac{1}{K+1}\right)\right) \\ &\triangleq exp\left(j\frac{\pi d_\kappa l}{K-1}\right) \cdot exp\left(-j\frac{\pi d_\kappa l}{K+1}\right) \end{aligned} \tag{3.5}$$

Next, we investigate the construction of Fourier-based deterministic sensing matrix briefly for $p = 2$ and $p > 2$, respectively. More details could be found in [18].

Case 1: $p = 2$. In this case, each element of the row index set D in ***Construction 1*** is represented as

$$d_k \equiv -(k+1) \quad (\text{modulo } K+1)$$

for $0 \le k \le K-1$. Thus, $exp\left(j\frac{2\pi d_k t}{K+1}\right) = exp\left(-j\frac{2\pi(k+1)t}{K+1}\right)$ in (3.4). Consequently, we see that while t runs through 0 to K for given l, the $K+1$ column vectors of (3.4) ultimately form a $K \times (K+1)$ submatrix, where each row is from a $(K+$

1)-point DFT matrix excluding the row with all one, and then masked by $\gamma_{\kappa}^{(l)}$ of (3.5). In addition, if l runs through 0 to $K+2$, then we will obtain $K-1$ submatrices and a variant $\mathbf{A}'$ by concatenating them.

Case 2: $p > 2$. In this case, we modify the index set $D = \{d_0, \cdots, d_{K-1}\}$ by adding $\frac{k+1}{2}$. Then the row indices will be reordered as

$$d_k{}' = \begin{cases} d_{k+\frac{k+1}{2}}, & 0 \le k < \dfrac{K-1}{2} \\ d_{k-\frac{k-1}{2}}, & \dfrac{K-1}{2} \le k < K-1 \end{cases}$$

$$\equiv -(k+1) \quad (\text{modulo } K+1), \ 0 \le k \le K-1$$

From the equation above, we have $exp\left(j\frac{2\pi d_k{}'t}{K+1}\right) = exp\left(-j\frac{2\pi(k+1)t}{K+1}\right)$ for the permuted row indices. Therefore, it is also clear that while t runs through 0 to K for given l, the $K+1$ column vectors of (3.4) with row indices $d_k{}'$ also form a $K \times (K+1)$ DFT-based submatrix, where each row is from a $(K+1)$-point DFT matrix excluding with the row with all one, and then masked by a constant factor.

Lemma 1: The $K \times N$ sensing matrix $\mathbf{A}$ in ***Construction 1*** has the following properties.

1) The coherence is $1/\sqrt{K}$

2) A pair of rows is mutually orthogonal, so $\mathbf{A}$ forms a tight frame.

3) All the row sums are equal to zero.

Proof: [20] From Proposition 1 and Theorem 2 of [12], it is easily checked that 1) is true. In addition, a pair of rows in each submatrix $\sigma^{(l)}$ is mutually orthogonal from the DFT-based structure with constant row mask vectors. Therefore, 2) is also true in concatenating the L DFT-based submatrices. In ***Construction 1***, (3.1) and (3.2)

ensure that no submatrix of $\mathbf{A}$ has all one row masked by a constant factor, which, due to the DFT-based structure, concludes that all the row sums of each submatrix are equal to zero. Thus, 3) is true from the concatenation. Also, these three properties have been tested and proved in the numerical way. Therefore, the main purpose of *Lemma 1* is to prove that Fourier-based deterministic sensing matrix $\mathbf{A}$ requires the statistical restricted isometry property (StRIP).

3.2 Statistical Restricted Isometry Property for A

Calderbank et al. demonstrated a statistical method in [6] to show that a deterministic sensing matrix is new-isometry on s-sparse vectors with high probability in the uniform distribution. Precisely, a $K \times N$ Fourier-based deterministic sensing matrix $\mathbf{A}$ requires the statistical restricted isometry property (StRIP) as derived from Section 2.6.

Corollary1[18]: *Let* $\frac{s-1}{N-1} < \epsilon < 1$. *There exists a constant* c *such that if the sparsity level* s *satisfies* $s \leq \frac{\epsilon^2}{C} \cdot \frac{K}{\log N}$, *then* $\mathbf{A}$ *in* ***Construction 1*** *has the StRIP with probability exceeding* $1 - \delta$, *or*

$$\Pr\left(\left|\left|\mathbf{Ax}\right|\right|^2 - \left|\left|\mathbf{x}\right|\right|^2\right| \leq \epsilon\left|\left|\mathbf{x}\right|\right|^2\right) \geq 1 - \delta$$

with respect to a uniform distribution of the vectors $\mathbf{x}$ *among all* s*-sparse vectors in* $\mathbb{R}^N$, *where* $\delta = 4\,exp\left[-\frac{\left(\epsilon-\left(\frac{s-1}{N-1}\right)\right)^2 \cdot K}{32s}\right]$. *Additionally, unique sparse reconstruction is guaranteed with probability exceeding* $1 - \delta$.

Remark 3: As stated in Remark 12 of [6], if $s = O(K/\log N)$, then unique sparse recovery is guaranteed with probability $1 - N^{-1}$ for sparse signals with

uniform distribution

3.3 FFT-based Signal Measurement and Recovery

In this section, we discuss the measurement and recovery processes of deterministic compressed sensing with the matrix $\mathbf{A}$ in ***Construction 1***. The Fourier-based deterministic sensing matrix $\mathbf{A}$ has the structure of DFT-based submatrix, the fast Fourier transform (FFT) technique can thus be used in the processes.

3.3.1 Measurement

The measurement process of compressed sensing is $\mathbf{y} = \mathbf{A}\mathbf{x}$, where $\mathbf{x} = (x_0, \cdots, x_{N-1}) \in \mathbb{R}^N$ and $\mathbf{y} = (y_0, \cdots, y_{K-1}) \in \mathbb{C}^K$. Due to the $K \times N$ sensing matrix $\mathbf{A}$ contains L distinct $(K+1)$-point DFT-based submatrices, the efficient FFT algorithm can be applied to the measurement process.

For $b = K + 1$, let $\mathrm{x}_l = (x_{bl}, \cdots, x_{bl+b-1})$ be a segment of $\mathbf{x}$ of length b, where $0 \leq l \leq L - 1$. Let $\tilde{x}_k^{(l)}$ be the b-point DFT of x_l, i.e.,

$$\tilde{x}_k^{(l)} = \sum_{t=0}^{b-1} x_{bl+t} e^{-j\frac{2\pi tk}{b}}, \quad 0 \leq k \leq b-1 \tag{3.6}$$

For fast implementation, we can employ this FFT algorithm to the L distinct segments of $\mathbf{x}$ in parallel at the same time. For each l, let $\boldsymbol{X}_k^{(l)} = \tilde{x}_{k+1}^{(l)}$ for $0 \leq k \leq K-1$. From (3.1) and (3.2), we can easily check for the two cases below

a. $p = 2$,

$$\mathbf{y}_k = \frac{1}{\sqrt{K}} \sum_{l=0}^{L-1} \boldsymbol{X}_k^{(l)} \gamma_k^{(l)}, \qquad 0 \le k \le K-1 \tag{3.7}$$

b. $p > 2$,

$$\mathbf{y}_k = \begin{cases} \frac{1}{\sqrt{K}} \sum_{l=0}^{L-1} \boldsymbol{X}_k^{(l)} \gamma_{k+\frac{K+1}{2}}^{(l)}, & 0 \le k < \frac{K-1}{2} \\ \frac{1}{\sqrt{K}} \sum_{l=0}^{L-1} \boldsymbol{X}_k^{(l)} \gamma_{k-\frac{K-1}{2}}^{(l)}, & \frac{K-1}{2} \le k < K-1 \end{cases} \tag{3.8}$$

Figure 3.2 below illustrates how we apply the FFT algorithm to the Fourier-based deterministic sensing matrix $\mathbf{A}$ with $p = 2$ in ***Construction 1***, where $0 \le l \le L-1$. For the case of $p > 2$, changing the order of row indices yields a similar process.

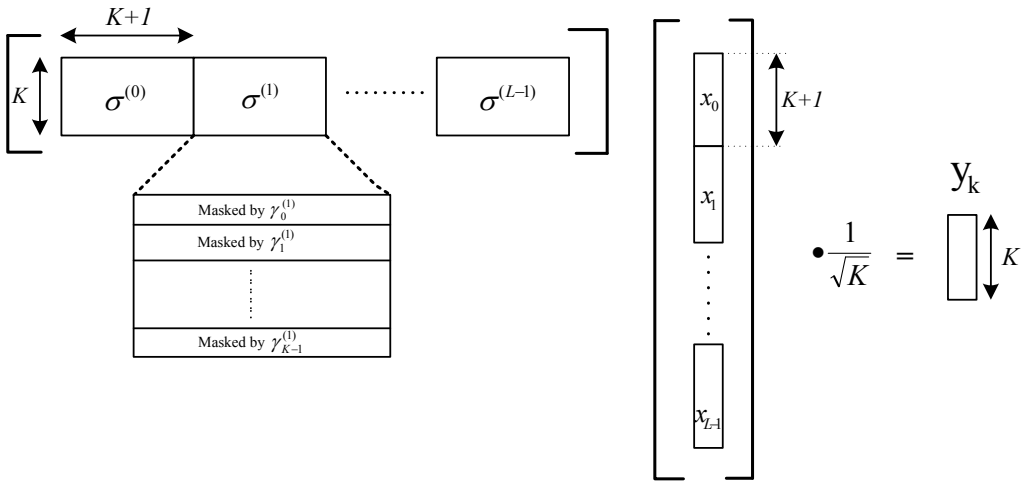

Figure 3.2 The signal measurement with FFT algorithm

3.3.2 Reconstruction

For the input s-sparse signal reconstruction, we apply the CoSaMP algorithm described in Algorithm 2.1 of [21], which is summarized in Table 2.2 and the process details explained in CoSaMP recovery algorithm of Chapter 2.

In Table 2.2, a signal proxy is $\mathbf{f} = \mathbf{A}^H\mathbf{v} = (f_0, \dots, f_{N-1})$, where the sample vector shown as $\mathbf{v} = (v_0, \dots, v_{K-1})$ and $\mathbf{A}^H$ represents the complex conjugate of $\mathbf{A}$. $\mathbf{v}$ is initializing as a (noisy) measurement vector **u.** Particularly, noiseless measurement is showing as $\mathbf{v} = \mathbf{u}$. At each iteration, the residual $\mathbf{v}$ will be updated as $\mathbf{v} = \mathbf{u} - \mathbf{A}\hat{\mathbf{x}}_t$, where $\hat{\mathbf{x}}_t$ is an estimate s-sparse vector of $\mathbf{x}$ at tth iteration. The matrix-vector multiplication for $\mathbf{f}$ can be achieved by the FFT algorithm due to the structure of the submatrices in $\mathbf{A}$. Because we applied the mask vector $\gamma_\kappa^{(l)}$ to the Fourier-based deterministic sensing matrix $\mathbf{A}$. First, we create a de-masked version of $\mathbf{v}$ of length $K+1$, i.e., $\tilde{\mathbf{v}}^{(l)} = \left(\tilde{v}_0^{(l)}, \dots, \tilde{v}_K^{(l)}\right)$, where $\tilde{v}_0^{(l)} = 0$, and if $p = 2$,

$$\tilde{v}_{k+1}^{(l)} = v_k \cdot \gamma_k^{(l)^*}, \qquad 0 \le k \le K-1 \tag{3.9}$$

or if $p > 2$,

$$\tilde{v}_{k+1}^{(l)} = \begin{cases} v_k \cdot \gamma_{k+\frac{K+1}{2}}^{(l)^*}, & 0 \le k < \dfrac{K-1}{2} \\ v_k \cdot \gamma_{k-\frac{K-1}{2}}^{(l)^*}, & \dfrac{K-1}{2} \le k < K-1 \end{cases} \tag{3.10}$$

Then, applying the b-point IDFT to $\tilde{\mathbf{v}}^{(l)}$ yields a segment of $\mathbf{f}$ of length $b = K+1$, i.e., $\tilde{\mathbf{f}}_l = (f_{bl}, \dots, f_{bl+b-1})$ where

$$f_{b\ell+t} = \frac{1}{\sqrt{K}} \sum_{k=0}^{b-1} \tilde{v}_k^{(l)} e^{j\frac{2\pi tk}{b}} \tag{3.11}$$

where $0 \le t \le b-1$. For fast implementation, the FFT algorithm can be applied to the L distinct demasked versions of $\mathbf{v}$ simultaneously in a parallel fashion. Finally, concatenating L segments forms $\mathbf{f} = \left(\tilde{\mathbf{f}}_0|, \dots, |\tilde{\mathbf{f}}_{L-1}\right)$**.** For $p = 2$, Figure 3.3 below shows the signal reconstruction with FFT algorithm for Fourier-based deterministic matrix $\mathbf{A}$, where $0 \le l \le L-1$. Also, for the case of $p > 2$, a similar process can be produced by changing the order of row indices

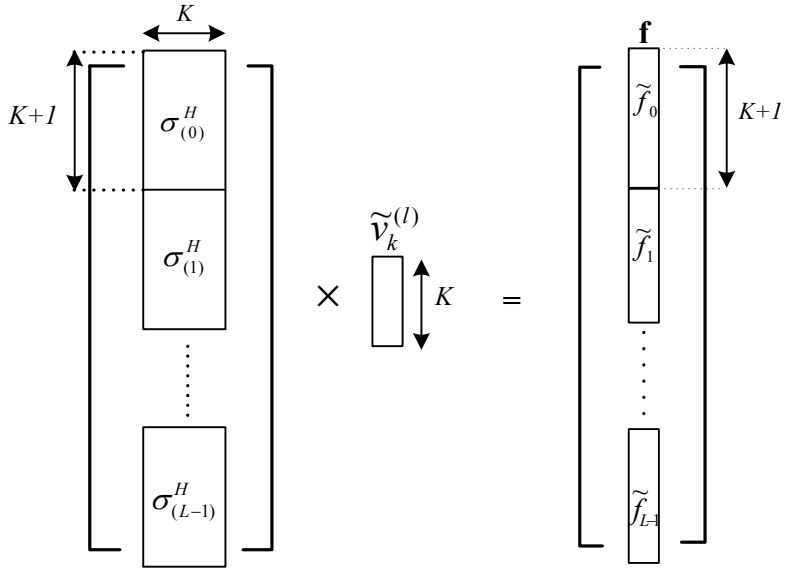

Figure 3.3 The signal reconstruction with FFT algorithm

Along with updating current samples at each iteration, the matrix-vector multiplication of $\mathbf{A}\hat{\mathbf{x}}_t$ is also accomplished by using the FFT algorithm with a similar approach in the measurement process. The halting criterion of the CoSaMP algorithm is if the norm of updated samples is sufficiently small or the iteration counter reaches the sparsity level.

Table 1 of [21] discussed that forming a signal proxy, the cost of the matrix-vector multiplication plays a main role in the algorithm complexity. Consequently, each iteration of the FFT-based CoSaMP recovery algorithm requires the complexity of $O(L \cdot b \log b) \approx O(N \log K)$.

Chapter 4

Empirical Experiments

In this section, we compare the reconstruction performances of CoSaMP and OMP recovery algorithms with Fourier-based deterministic sensing matrices **A**. Then, the Fourier-based deterministic sensing matrices are compared to chirp sensing codes [7] and random partial Fourier sensing matrices in terms of the empirical recovery performance with noiseless, noisy scenarios and image processing. Table 4.1 summarized various parameters of $K = p^r$ have been used in our experiments. Other prime parameters can be considered as well. In the experiments, we set $N = (K + 1)L$ for $L = 4$ and 8 for the Fourier-based deterministic sensing matrices. All the experiments are completed in MATLAB.

Table 4.1 Various parameters of $K = p^r$ in the experiments

p	r	K
2	6	64
	7	128
	8	256
3	4	81
5	3	125
7	3	343

4.1 Comparison between OMP and CoSaMP

Compressive sampling matching pursuit (CoSaMP) is the recovery algorithm which is ultimately based on the Orthogonal Matching Pursuit (OMP). The CoSaMP can also be treated as the extension version of OMP. In [44], OMP reconstructs $\mathbf{x}$ after s iterations, except with probability N^{-1}. In this setting, OMP might fail for some sparse signals, so it does not provide the same uniform guarantees as convex relaxation [46]. The CoSaMP algorithm, however, uses the restricted isometry properties of the sampling matrix to ensure that the identification step is successful. Figure 4.1 and Figure 4.2 show the comparison performance in successful recovery rate between CoSaMP and OMP algorithms incorporating with the Fourier-based deterministic sensing matrix when $L = 4$ and $L = 8$, respectively. In our measurement process, each nonzero entry of an s-sparse signal $\mathbf{x} \in \mathbb{R}^N$ has the magnitude of 1,where its position and sign are chosen uniformly at random. For signal recovery, these two recovery algorithms are applied to total 2000 sample vectors measured by the Fourier-based deterministic sensing matrix. Moreover, the halting criterion of CoSaMP algorithm can be triggered if the updated samples is very small, i.e., $\|\mathbf{v}\| < 10^{-4}$ or the iteration reaches the sparsity level s. However, OMP reconstructs the input signal $\mathbf{x}$ after s iterations.

In the experiments, we set $N = (K + 1)L$ when $L = 4$ and 8 for the Fourier-based deterministic sensing matrices. Figure 4.1 shows the comparison results with $(K, N) = (81,328)$ when $L = 4$. In figure 4.2, result is displayed with $(K, N) = (256,2056)$ when $L = 8$. Apparently, from the Figure 4.1, CoSaMP algorithm demonstrates much higher recovery rate than OMP at small sparsity levels when $L = 4$. Also, we can easily check that CoSaMP shows much better recovery performance than OMP when $L = 8$ in Figure 4.2. We believe that the reason why CoSaMP outperforms OMP in this scenario is that it has more sophisticated selection rule which will be led to find the nonzero entries more accurately.

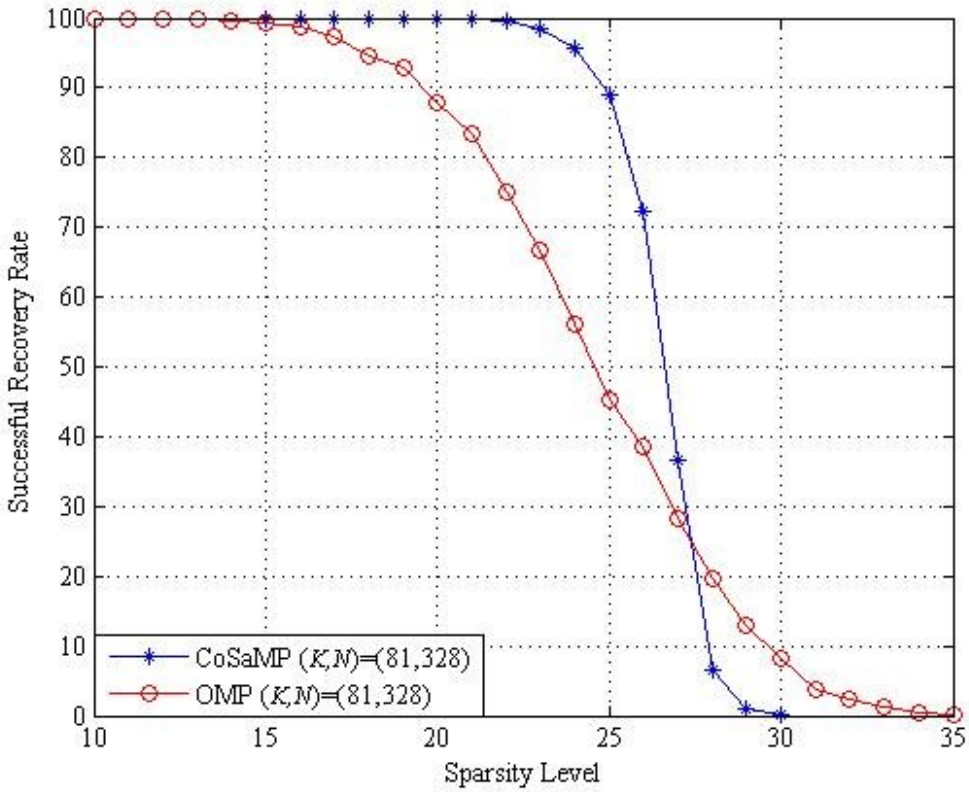

Figure 4.1 The comparison between CoSaMP and OMP in successful recovery rate when $L = 4$.

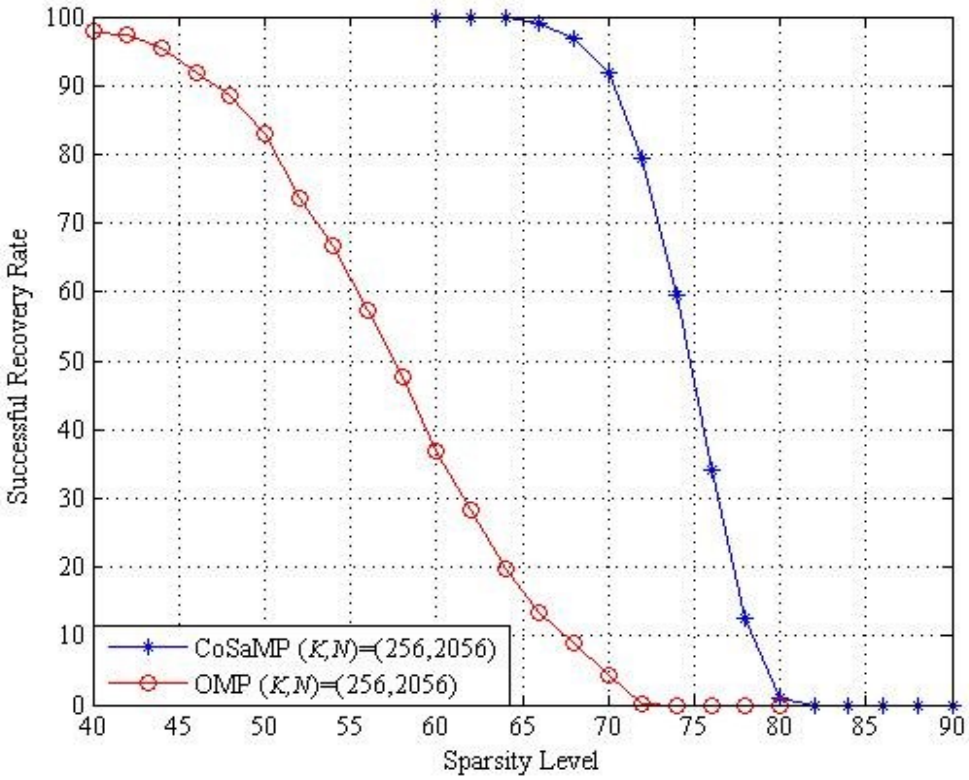

Figure 4.2 The comparison between CoSaMP and OMP in successful recovery rate when $L = 8$.

4.2 Recovery Performance for Compressed Sensing

In the experiments, we set $L = 4$ and 8 for the Fourier-based deterministic sensing matrices. We then chose several parameters from the Table 4.1 by using $K = 3^4 = 81$ and $N = (K + 1)L = 328$ for $L = 4$, while $K = 2^8 = 256$ and $N = (K + 1)L = 2056$ for $L = 8$. A random partial Fourier matrix has the

same parameters of K and N as Fourier-based deterministic sensing matrix for comparison. To obtain it, we made 10 trials to select K rows randomly from the N-point IDFT matrix, where the coherence was checked at each trial. Then, we chose the one with the smallest coherence for our experiments. For a chirp sensing matrix, K has to be set as a prime number [7] close to the parameter used for the Fourier-based deterministic sensing matrix, and $N = KL$ for $L = 4$ and 8. Precisely, $(K, N) = (79, 316)$ for $L = 4$, and $(K, N) = (257, 2056)$ for $L = 8$, respectively. To guarantee the UStRIP, each submatrix of the partial chirp sensing matrix has an alternating polarity as in [36]. Similarly, we also show the results of Fourier-based deterministic sensing matrix and random partial Fourier sensing matrix with $(K, N) = (128, 520)$, for $L = 4$, and $(K, N) = (125, 1008)$, for $L = 8$. To be compared, the parameters of chirp sensing codes are correspondingly set to $(K, N) = (127, 506)$, and $(K, N) = (127, 1016)$, respectively. Besides the above parameters, we also checked the empirical recovery performance with other parameters of $(K, N) = (64, 260)$, $(343, 2752)$ for the Fourier-based deterministic sensing matrices and random partial Fourier sensing matrices, and $(K, N) = (61, 244)$, $(337, 2696)$ for chirp sensing codes, respectively

In this measurement process, each nonzero entry of an s-sparse signal $\mathbf{x} \in \mathbb{R}^N$ has the magnitude of 1,where its position and sign are chosen uniformly at random. For signal recovery, the FFT-based CoSaMP reconstruction algorithm is applied to total 2000 sample vectors measured by the three sensing matrices. In Table 2.2, the recovery algorithm is stopped if $||\mathbf{v}|| < 10^{-4}$ or the iteration counter reaches the sparsity level s. A success is declared in reconstruction if the estimate error is reasonably small for the estimate $\hat{\mathrm{x}}$, i.e., $||\mathbf{x} - \hat{\mathbf{x}}|| < 10^{-6}$.

4.2.1 Successful Recovery Rate with Noiseless Signals

Figures 4.3 and 4.4 display successful recovery rate of the three sensing matrices from noiseless measurements for $L = 4$ and 8, respectively. In the figures, the Fourier-based deterministic sensing matrices have the slightly higher recovery rates than random partial Fourier matrices. Figures 4.3(a) and 4.3(b) show that the successful recovery rate of Fourier-based deterministic sensing matrix is obviously higher than that of the chirp sensing code. In the Figure 4.4 (a), the results can be clearly shown that the chirp sensing codes have an outstanding performance than Fourier-based deterministic sensing matrix and random partial Fourier sensing matrix. However, we believe that the difference occurred because of the larger parameter K of the chirp sensing code. In the case of $(K, N) = (256, 2056)$ from Figure 4.4 (b), it is revealed almost the same recovery performance with three sensing matrices. We made a similar observation from the other parameters that the Fourier-based deterministic sensing matrices outperform random partial Fourier matrices, but show almost the same recovery rates as chirp sensing codes.

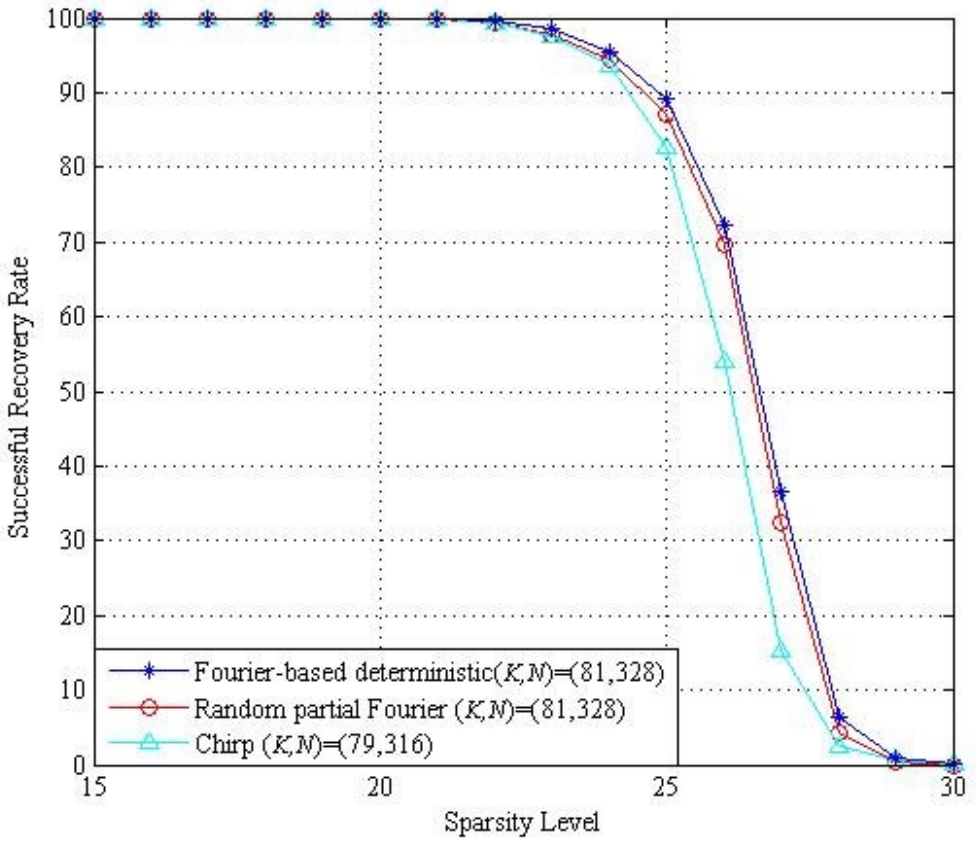

(a) $(K, N) = (81, 328)$

Figure 4.3 Successful recovery rates of Fourier-based deterministic, random partial Fourier and chirp sensing matrices for $L = 4$ from noiseless measurement

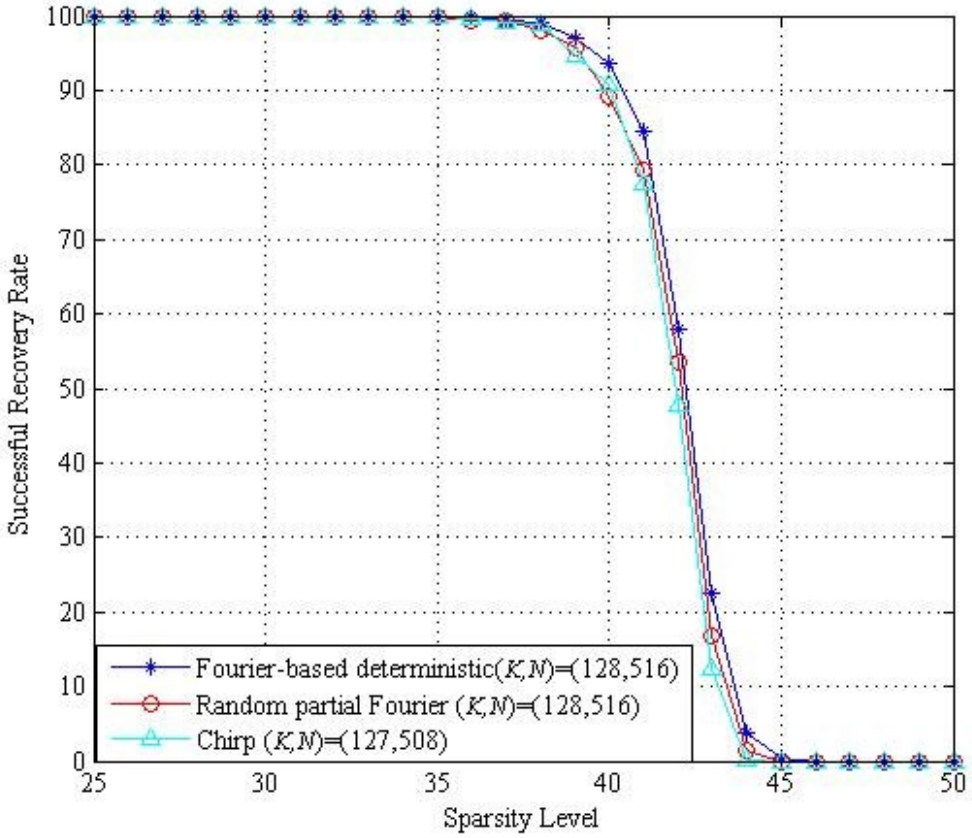

(b) $(K, N) = (128, 516)$

Figure 4.3 Successful recovery rates of Fourier-based deterministic, random partial Fourier and chirp sensing matrices for $L = 4$ from noiseless measurement

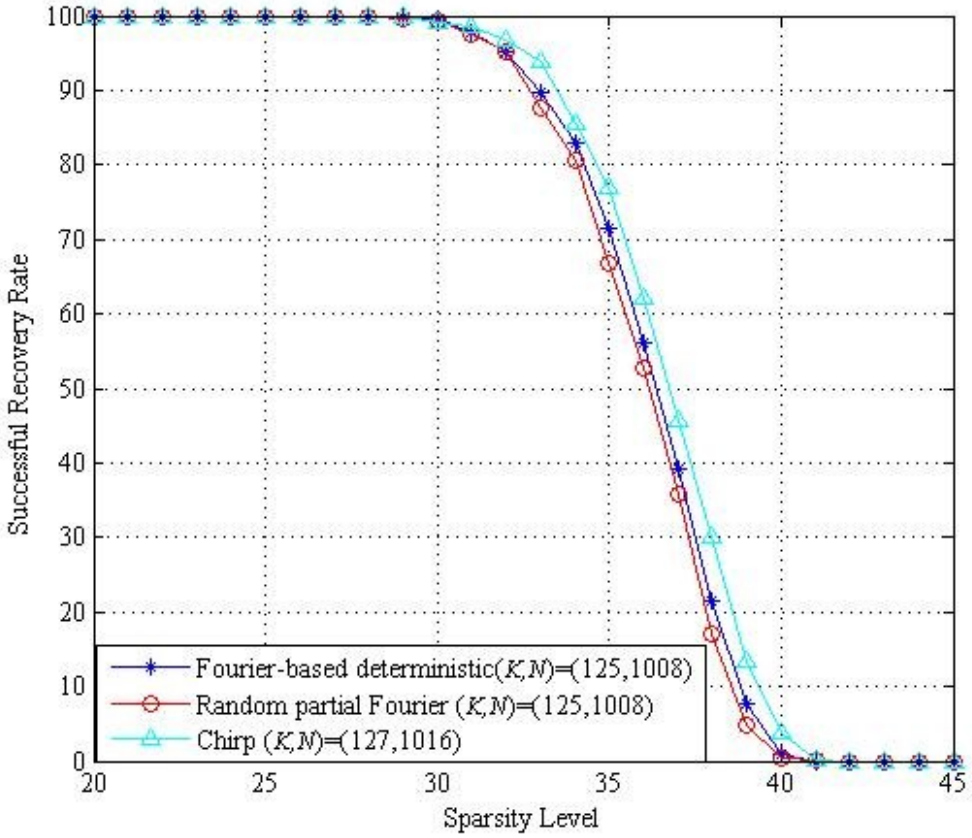

(a) $(K, N) = (125, 1008)$

Figure 4.4 Successful recovery rates of Fourier-based deterministic, random partial Fourier and chirp sensing matrices for $L = 8$ from noiseless measurement

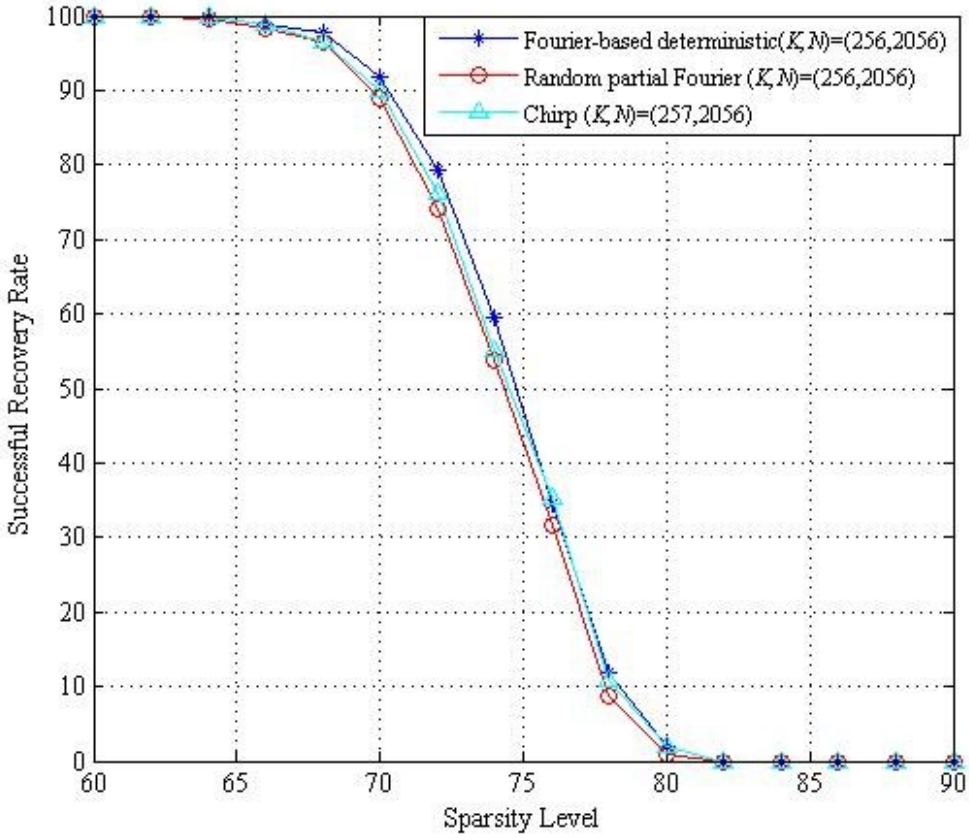

(b) $(K, N) = (256, 2056)$

Figure 4.4 Successful recovery rates of Fourier-based deterministic, random partial Fourier and chirp sensing matrices for $L = 8$ from noiseless measurement

4.2.2 Reconstruction SNR with Noiseless Signals

Now, we continue to test the recovery performance of Fourier-based deterministic sensing matrices from the reconstruction SNR for noiseless case to compare with chirp sensing codes and random partial Fourier matrix. Then, we define the reconstruction SNR as

$$\mathrm{SNR}_{\mathrm{reconst}}(\mathrm{dB}) = 10\log_{10}\frac{\|\mathbf{x}\|^2}{\|\mathbf{x}-\hat{\mathbf{x}}\|^2} \quad , \tag{4.1}$$

where $\mathbf{x}$ is an original sparse signal and $\hat{\mathbf{x}}$ is its estimate from reconstruction. The reconstruction SNR is computed in average sense over all tested signals for a given sparsity level. From Figures 4.5 and 4.6, they show that Fourier-based deterministic sensing matrices have the slightly better performances than random partial Fourier sensing matrices, but the difference is not so significant. Again, the larger parameter K of the chirp sensing code seems to be the reason to make an outstanding performance in Figure 4.6(a). In the case of $(K, N) = (256, 2056)$, Figure 4.6 (b) displays almost the same recovery performance with three sensing matrices. We also observed the similar performance trend from other parameters that Fourier-based deterministic sensing matrices show almost the same reconstruction SNR as random partial Fourier and chirp sensing matrices in noiseless scenarios.

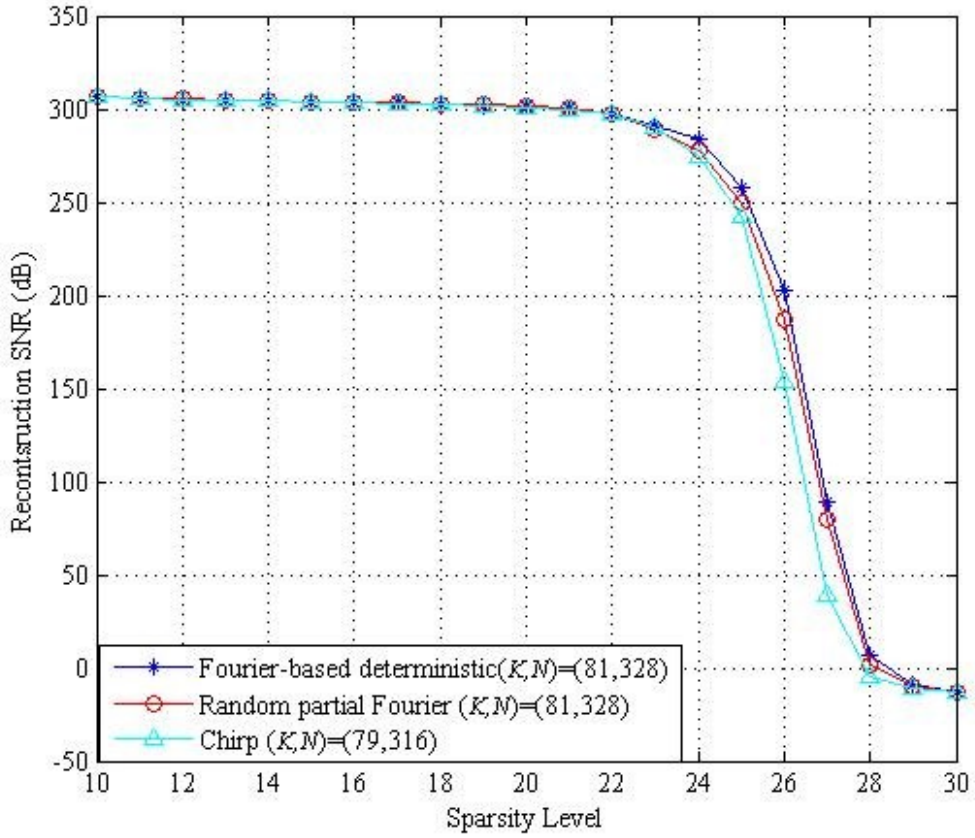

(a) $(K, N) = (81, 328)$

Figure 4.5 Reconstruction SNR of Fourier-based deterministic, random partial Fourier and chirp sensing matrices for $L = 4$ from noiseless measurement

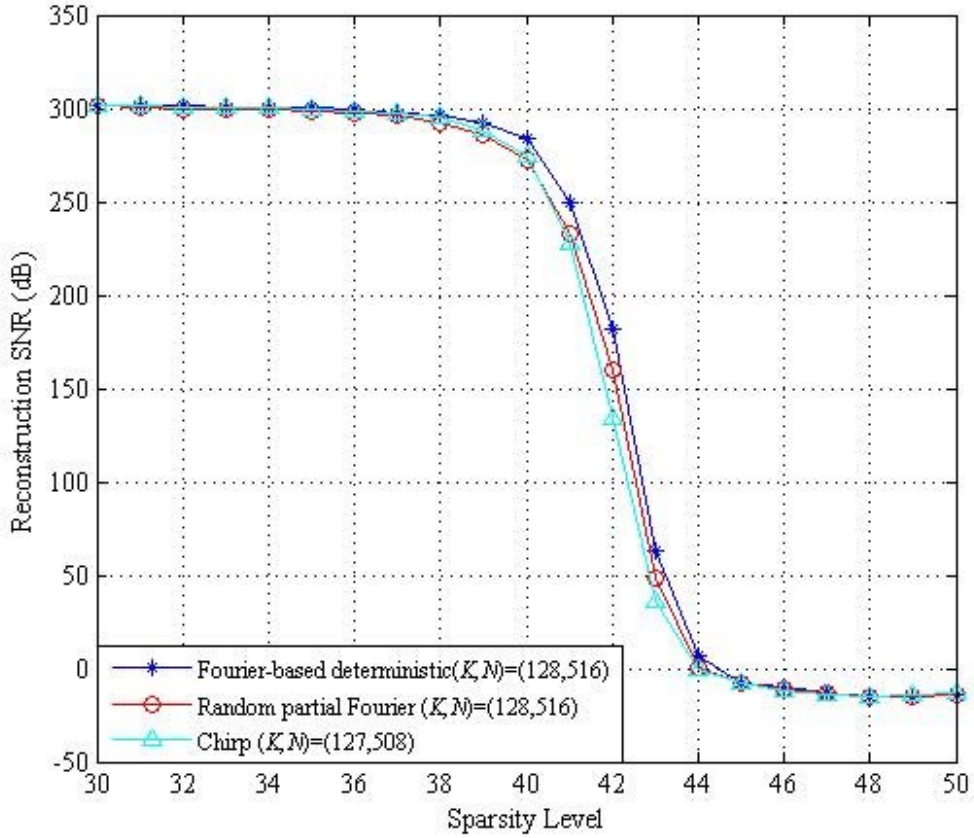

(b) $(K, N) = (128, 516)$

Figure 4.5 Reconstruction SNR of Fourier-based deterministic, random partial Fourier and chirp sensing matrices for $L = 4$ from noiseless measurement

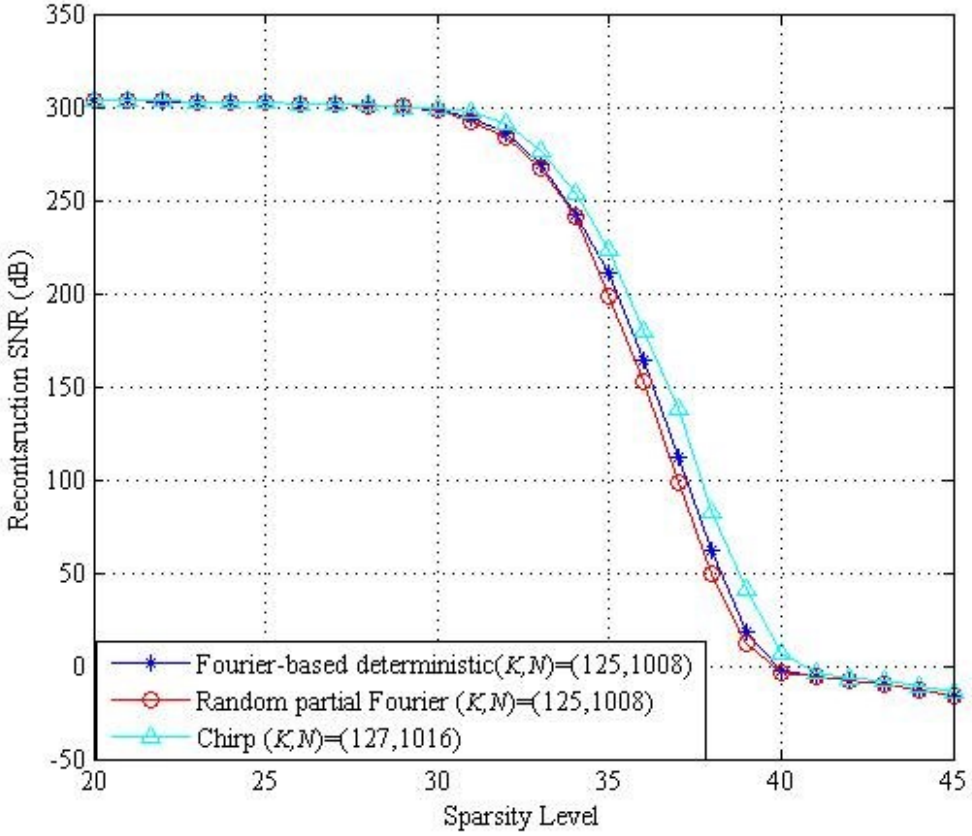

(a) $(K, N) = (125, 1008)$

Figure 4.6 Reconstruction SNR of Fourier-based deterministic, random partial Fourier and chirp sensing matrices for $L = 8$ from noiseless measurement.

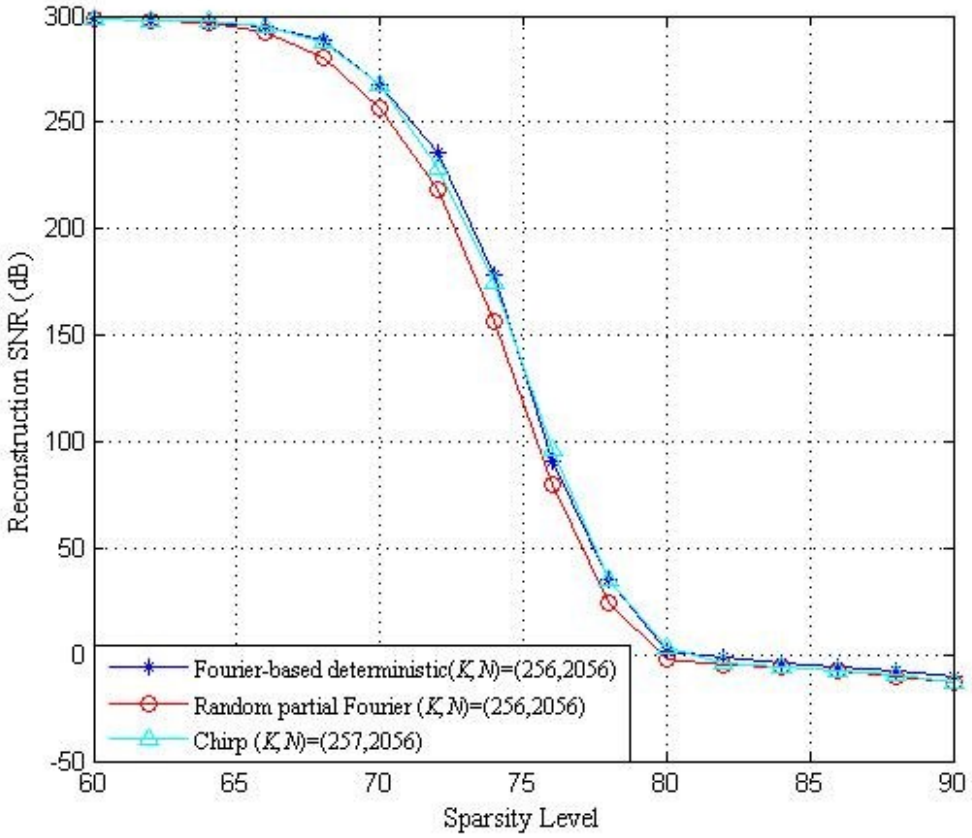

(b) $(K, N) = (256, 2056)$

Figure 4.6 Reconstruction SNR of Fourier-based deterministic, random partial Fourier and chirp sensing matrices for $L = 8$ from noiseless measurement.

4.3 Recovery Performance for Noisy Compressed Sensing

4.3.1 Reconstruction SNR with Noisy Signals

In the noisy compressed sensing, the noisy measurement is represented as $\mathbf{u} = \mathbf{y} + \mathbf{z} = \mathbf{A}\mathbf{x} + \mathbf{z}$, where $\mathbf{z}$ is the additive white Gaussian noise of zero mean and variance σ^2. Then, we can define the input SNR as follows:

$$\mathrm{SNR}_{\mathrm{input}}(\mathrm{dB}) = 10\log_{10}\frac{\|\mathbf{y}\|^2}{\sigma^2} \tag{4.2}$$

The input SNR is computed in average over all sample vectors. Also, the reconstruction SNR is defined in (4.1) to measure the recovery performance in noisy compressed sensing.

In this section, we consider the reconstruction performance from two aspects. First, Figures 4.7 and 4.8 sketch the reconstruction SNR of the three sensing matrices in Figures 4.3 and 4.4, respectively, from noisy measurements. In both figures, the input SNR is set as 15 dB. The figures revealed that Fourier-based deterministic sensing matrices outperform random partial Fourier and chirp sensing matrices at high sparsity levels, but the difference is negligible. Again, the smaller parameter K of the chirp sensing code seems to be the reason to make some difference in Figure 4.7. In addition, in Figure 4.8(a), due to the larger parameters, chirp sensing code presents relatively better performance. However, in the case of $(K, N) = (256, 2056)$, because the parameters in three sensing matrices are so close, Figure 4.8(b) displays almost the same recovery performance. The other parameters are also checked to get the similar performance trend that Fourier-based deterministic sensing matrices show almost the same reconstruction SNR as the others in noisy compressed sensing.

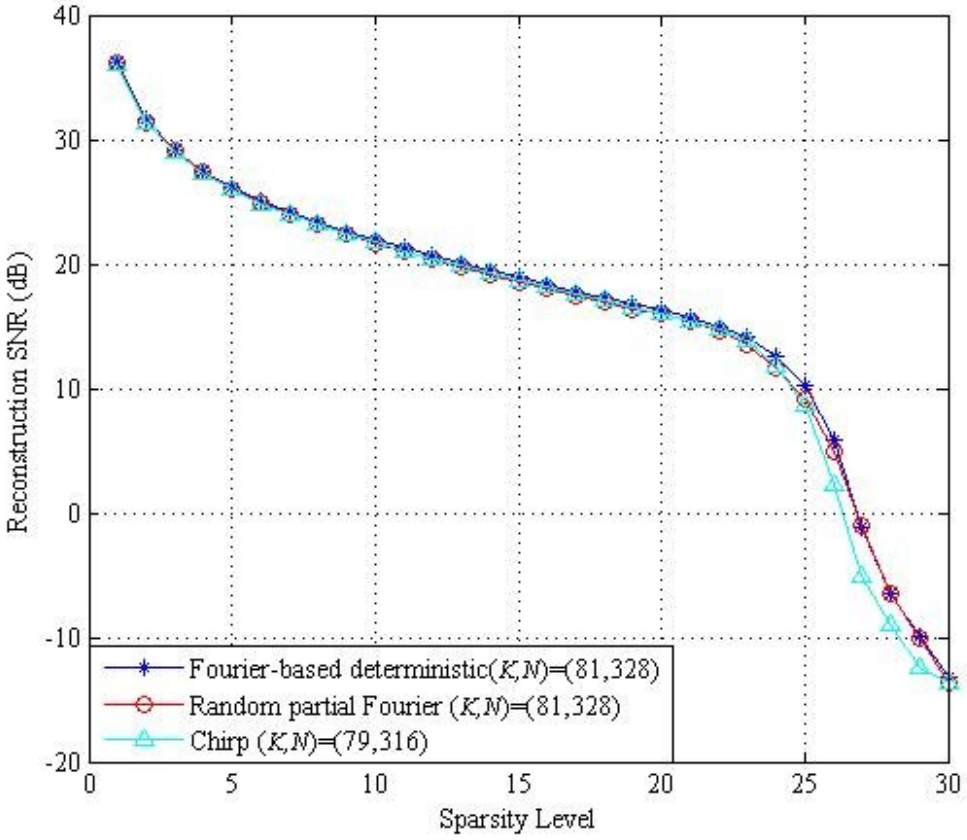

(a) $(\boldsymbol{K, N}) = (\mathbf{81, 328})$

Figure 4.7 Reconstruction SNR of Fourier-based deterministic, random partial Fourier and chirp sensing matrices in noisy compressed sensing for $L = 4$ with $\mathbf{SNR}_{input} = 15$ dB

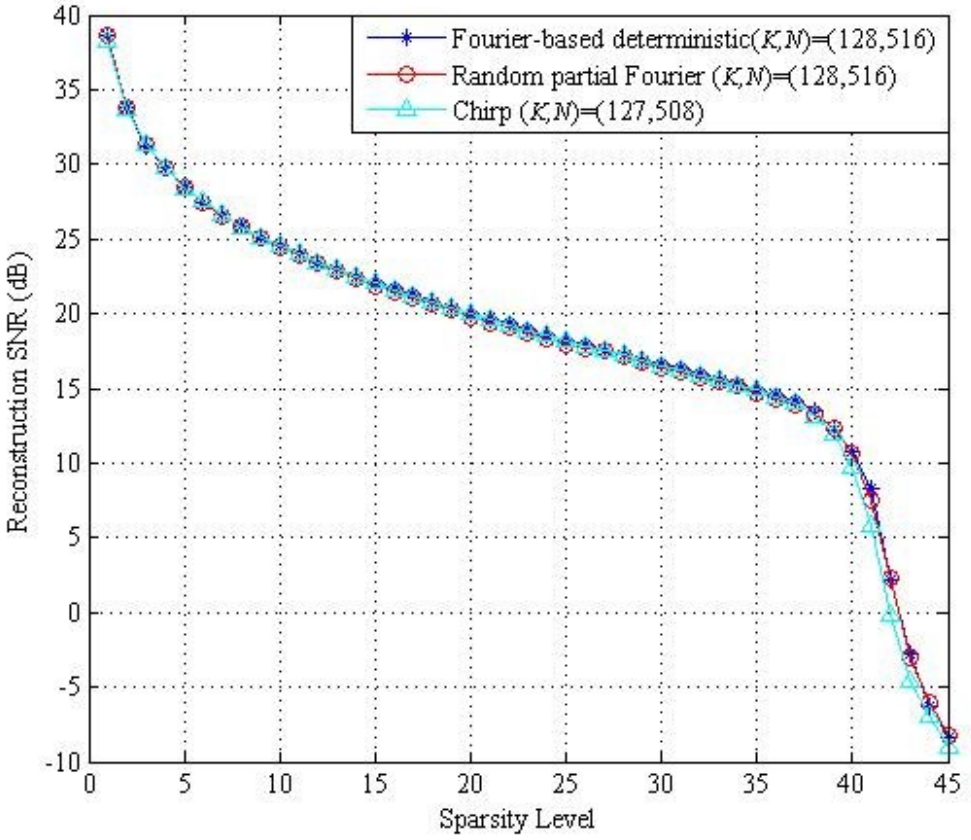

(b) $(K, N) = (128, 516)$

Figure 4.7 Reconstruction SNR of Fourier-based deterministic, random partial Fourier and chirp sensing matrices in noisy compressed sensing for $L = 4$ with $\text{SNR}_{input} = 15$ dB

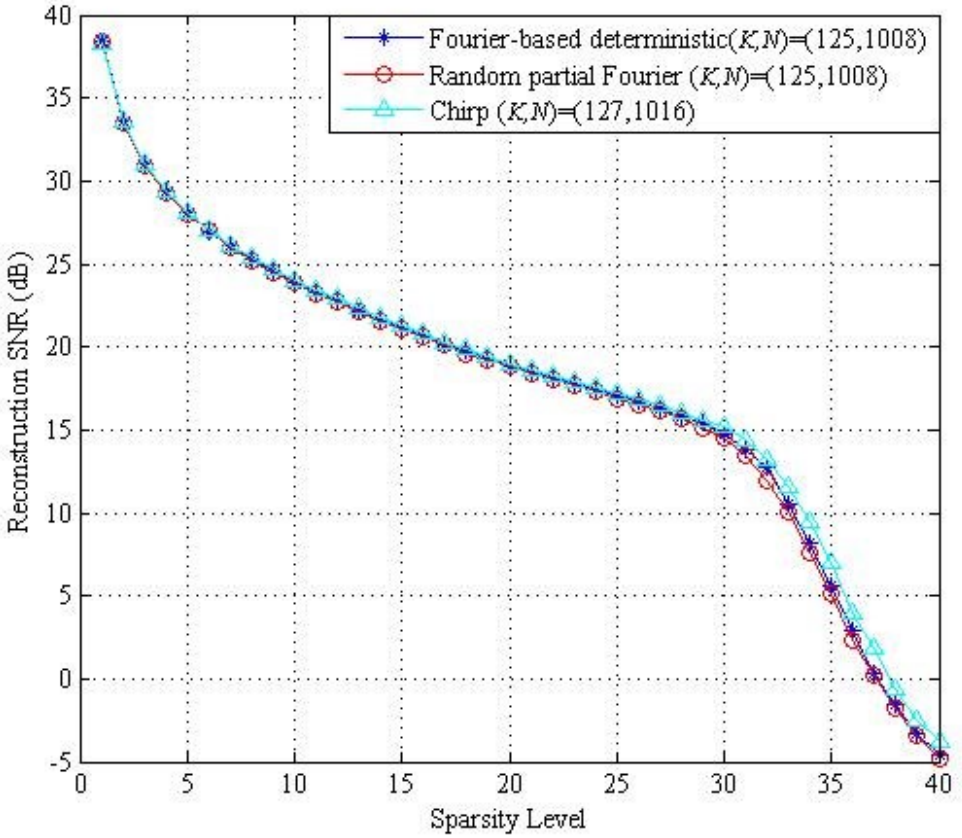

(a) $(K, N) = (125, 1008)$

Figure 4.8 Reconstruction SNR of Fourier-based deterministic, random partial Fourier and chirp sensing matrices in noisy compressed sensing for $L = 8$ with $\mathrm{SNR}_{input} = 15$ dB

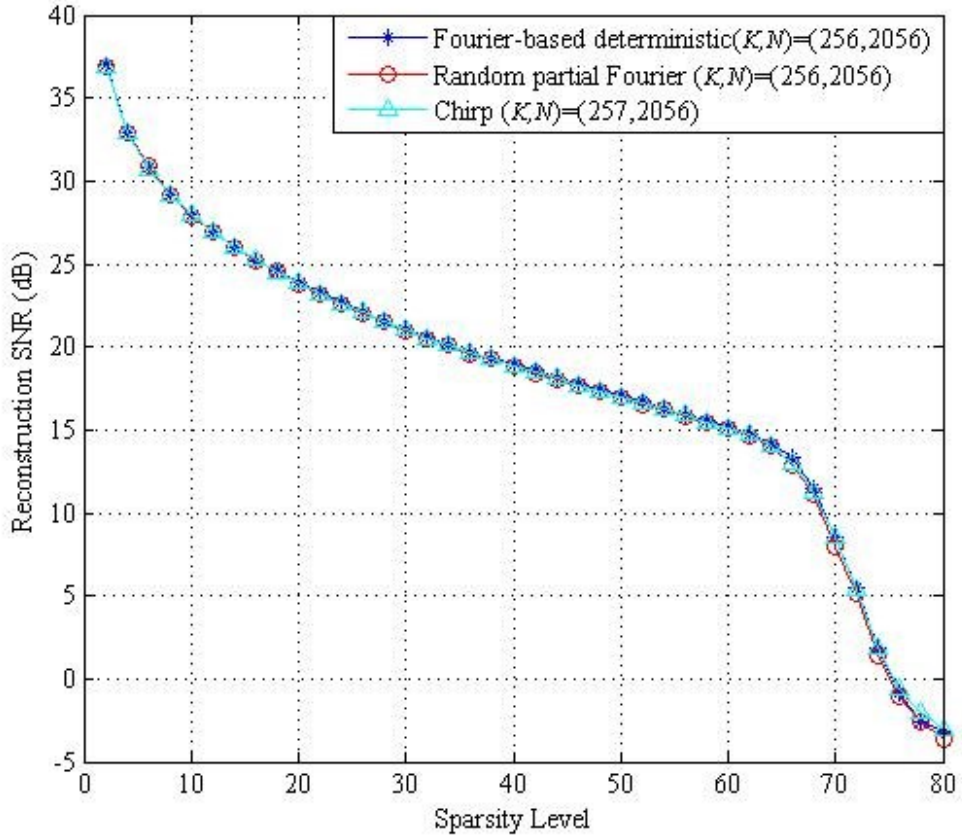

(b) $(K, N) = (256, 2056)$

Figure 4.8 Reconstruction SNR of Fourier-based deterministic, random partial Fourier and chirp sensing matrices in noisy compressed sensing for $L = 8$ with $\text{SNR}_{input} = 15$ dB

4.3.2 Reconstruction SNR vs. Input SNR

Figures 4.9 and 4.10 demonstrate reconstruction SNR versus input SNR of the three matrices by the parameters used in Figures 4.3 and 4.4, respectively in noisy compressed sensing. In Figure 4.9, it contains two sub figures, the sparsity levels of the original signals are set to 25 and 40 for $L = 4$, respectively. Similarly, 33-sparse and 70-sparse signals for $L = 8$ have been used in Figure 4.10. At the sparsity levels, we observed that the relationship between reconstruction and input SNR is linear for medium and high input SNR. In Figure 4.9, the chirp sensing code shows relatively worse relationship than the others, where the smaller parameters K seem to be the reason. Again, in Figure 4.10, chirp shows almost the same trend with Fourier-based deterministic sensing matrix, and they both display the better performance than random partial Fourier sensing matrix. To sum up, Fourier-based deterministic sensing matrices slightly outperform random partial Fourier matrices for high input SNR, but show almost the same trend with chirp sensing codes. Similar observations have been made from the other parameters.

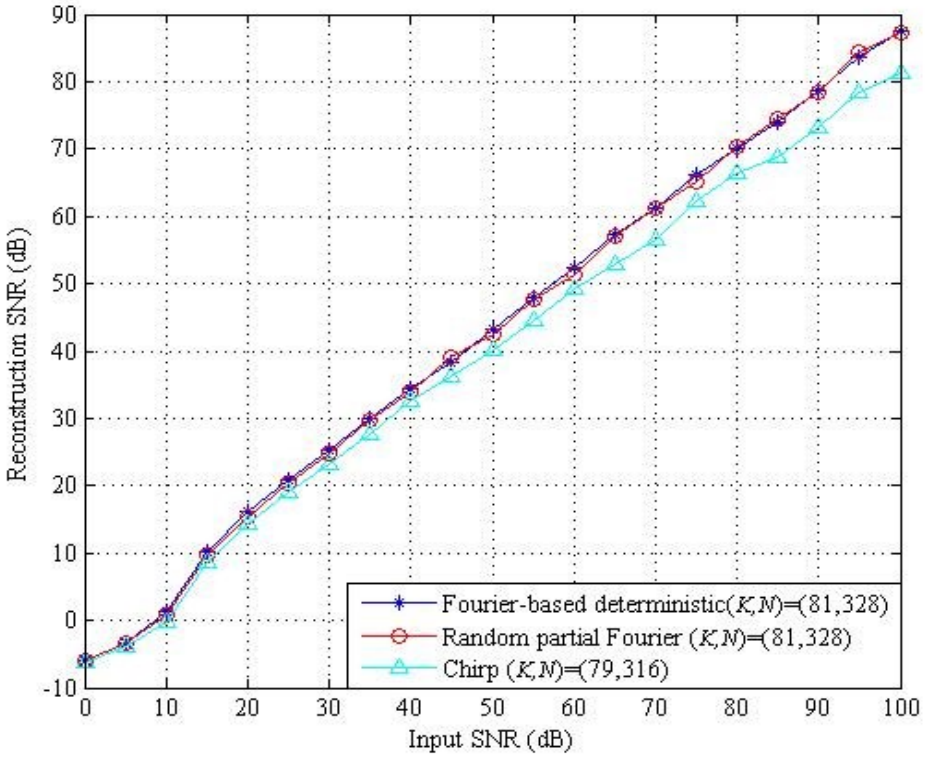

(a) $(K, N) = (81, 328)$

Figure 4.9 Reconstruction SNR versus input SNR in noisy compressed sensing for 25-sparse input signal when $L = 4$

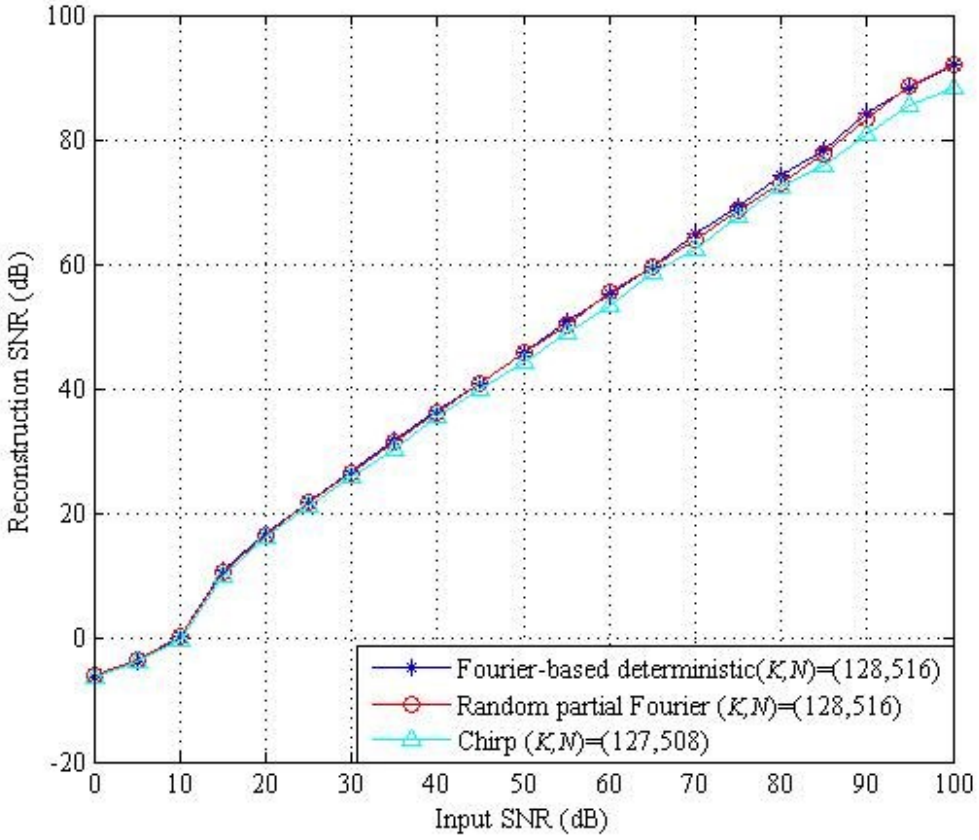

(b) $(K, N) = (128, 516)$

Figure 4.9 Reconstruction SNR versus input SNR in noisy compressed sensing for 40-sparse input signal when $L = 4$

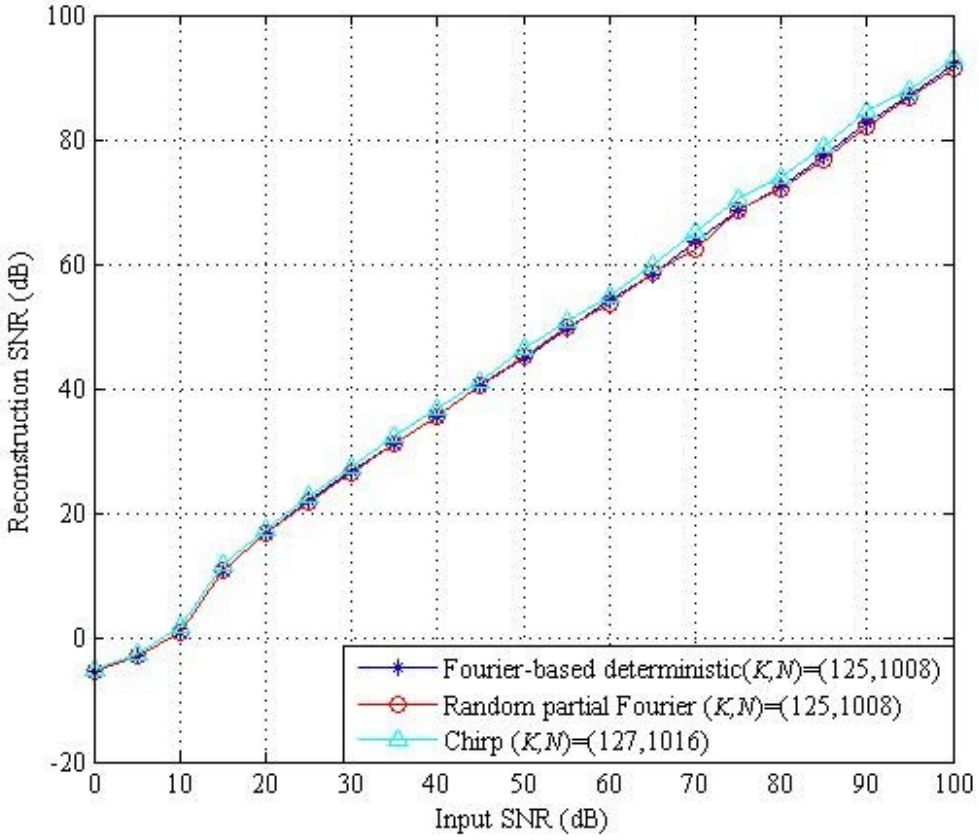

(a) $(K, N) = (125, 1008)$

Figure 4.10 Reconstruction SNR versus input SNR in noisy compressed sensing for 33-sparse input signal when $L = 8$

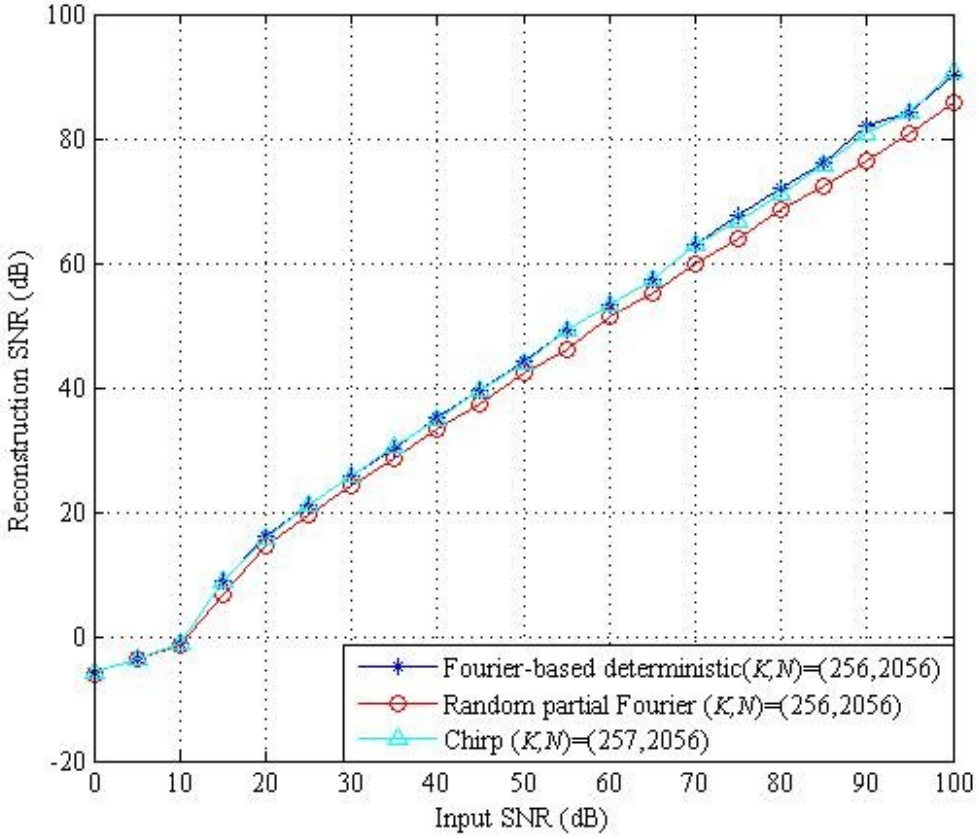

(b) $(\boldsymbol{K}, \boldsymbol{N}) = (\mathbf{256}, \mathbf{2056})$

Figure 4.10 Reconstruction SNR versus input SNR in noisy compressed sensing for 70-sparse input signal when $\boldsymbol{L} = \mathbf{8}$

4.4 Image Reconstruction

An original image of size 128×128 (or 256×256 and more) is sparsified by computing its Haar wavelet transform [30] and retaining a pre-determined fraction of its coefficients. In the sparsification, the largest coefficients of the pre-determined fraction must be kept, while the rest is set to zero. The process of sparsification of the original image is showing below.

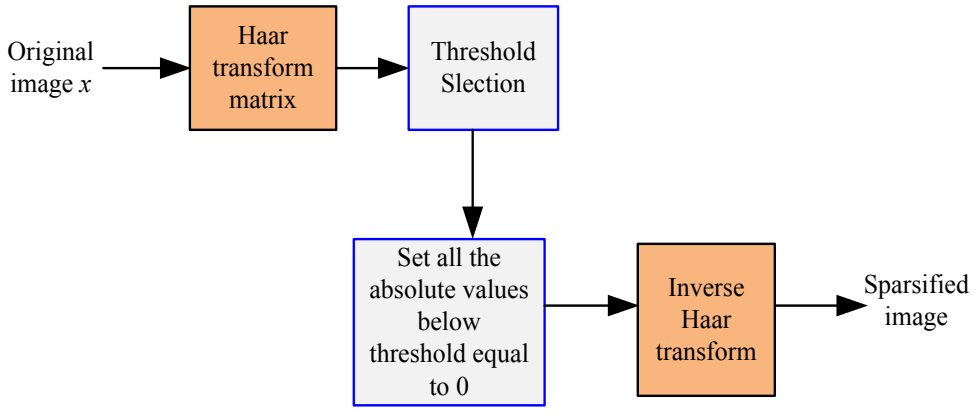

Figure 4.11 The process of image sparsification with Haar transform

According to the process of sparsification, an original 128×128 image and its corresponding sparsified image with the pre-determined sparsity can be shown below. Note that from Figure 4.12(b), we can observe that the relatively few wavelet coefficients are capturing the most of the signal energy. It also can show that many such images are highly compressible or sparse.

(a)

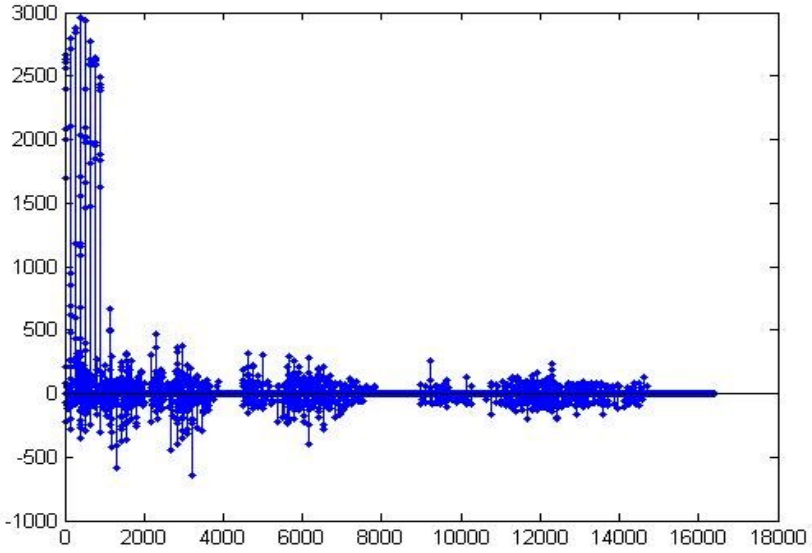

(b)

(c)

Figure 4.12 (a) an 128×128 original image; (b) its wavelet transform coefficients (arranged randomly); (c) The 7%- sparsified image

Then, the image data is measured with Fourier-based deterministic sensing matrix, random partial Fourier sensing matrix and chirp sensing code of the same size (for chirp with the closest prime number) and then reconstructed by CoSaMP recovery algorithm. In the noiseless measurement of an image, we set $p = 2$ and $L = 4$ for the three sensing matrix. Specifically, the compression rate $\left({}^{K}/_{N}\right)$ of an original image is set to 25% for 7%-sparse image in this experiment. To measure an $128 \times 128 = 2^{14}$ image, in our experiments, we can set $K = 2^{12}$ and $N = (K + 1)L = 2^{14} + 4$, where 4 additional zero bits can be appended to the original image. However, for the chirp sensing codes, the closest prime number to K should also be chosen, in our experiments, $K = 4093,\ N = 4K = 16372,$ where the 12 zero bits at the rear part should be discarded from the original image. Similarly, $K = 2^{10}$ and 2^{14} for 64×64 and 256×256 images can be considered, respectively. We present the comparison of 7% sparsified images. However, they look merely identical to reference image. From the reconstruction SNR as illustrates in Table 4.2, Fourier-based deterministic sensing matrix shows slightly better recovery performance, but the difference is neglect.

(a) Reference

(b) Fourier-based **(c) Random partial Fourier** **(d) Chirp**

Figure 4.13 Reconstructed images of 7% Cameraman with Fourier-based deterministic sensing matrices, random partial Fourier sensing matrices and chirp sensing codes look merely identical to the (sparsified) reference images

Table 4.2 The reconstruction SNR for 7% sparsified Cameraman

Sensing Matrix	Fourier-based deterministic	Random partial Fourier	Chirp
Reconstruction SNR (dB)	288.29	287.49	286.20

It is hard to see the difference from reconstructed images measured by the three sensing matrices. However, from the reconstruction SNR, we can see Fourier-based deterministic sensing matrices present a slightly better performance than random partial Fourier sensing matrices and chirp sensing codes, even though the differences are not so important. Overall, the empirical results in image reconstruction showed that Fourier-based deterministic sensing matrices guarantee the reliable recovery performance.

Chapter 5

Conclusions

This thesis has studied and analyzed the empirical recovery performance of Fourier-based deterministic sensing matrices. We first made experiments to compare the recovery performance of OMP and CoSaMP reconstruction algorithms with the deterministic sensing matrix. Based on the construction of Fourier-based deterministic sensing matrices, we deliberately built our experiments of deterministic compressed sensing, various $K = p^r$ and $N = (K + 1)L$ are possible for any prime p, and positive integers r and $L < K$. Therefore, a large number of sensing matrices with a variety of parameters can be provided for many applications in compressed sensing. In addition, an efficient and fast processing in signal recovery is possible from the DFT-based submatrix structure. By applying the FFT-based CoSaMP reconstruction algorithm, we compared Fourier-based deterministic sensing matrices with random partial Fourier sensing matrices and chirp sensing codes in noiseless and noisy scenarios, respectively. For image sparsification, we applied Haar wavelet transform to make an original image sparsified, and then the largest coefficients of original images were kept for the image reconstruction. The performance of Fourier-based deterministic sensing matrix was compared to random partial Fourier sensing matrix and chirp sensing code in image reconstruction. The empirical results revealed that the Fourier-based deterministic sensing matrices guarantee the reliable recovery performance.

In the future work, we will continue to focus on the image processing area by testing the different images with the larger size, for instance, 256×256, 512×512 or even bigger with different sparsity levels. Moreover, other input signals will be considered measuring by Fourier-based deterministic sensing matrices, such as the zero-mean real or complex valued input signals with Gaussian random distribution.

References

[1] D. L. Dohono, “Compressed sensing,” *IEEE Trans. Inform. Theory*, vol. 52, no. 4, pp. 1289 - 1306, Apr. 2006.

[2] E. Candès, J. Romberg, and T. Tao, “Robust uncertainty principles: exact signal reconstruction from highly incomplete information,” *IEEE Trans. Inform. Theory*, vol. 52, no. 2, pp. 489 - 509, Feb. 2006.

[3] E. Candès and T. Tao, “Near optimal signal recovery from random projections: universal encoding strategies”. *IEEE Trans. Inform. Theory*, vol. 52, no. 12, pp. 5406 - 5425, Dec. 2006.

[4] R. A. DeVore, “Deterministic constructions of compressed sensing matrices.” *J. of Complexity*, 23, pp. 918 - 925, Aug. 2007.

[5] H. Rauhut, “Compressive sensing and structured random matrices,” *Preprint*. May 2010.

[6] R. Calderbank, S. Howard, and S. Jafarpour, “Construction of a large class of deterministic sensing matrices that satisfy a statistical isometry property.” *IEEE J. Selected Topics in Signal Processing*, vol. 4, no. 2, pp. 358-374, Apr. 2010.

[7] L. Applebaum, S. D. Howard, S. Searle, and R. Calderbank, “Chirp sensing codes: deterministic compressed sensing measurements for fast recovery,” *Appl. Comput. Harmon. Anal. (ACHA)*, vol. 26, pp. 283-290, 2009.

[8] A. R. Calderbank, P. J. Cameron, W. M. Kantor, J. J. Seidel. “Z_4-Kerdock codes, orthogonal spreads, and external Euclidean line-sets.” *Processdings of the London Mathematical Society*- PROC

LONDON MATH SOC, vol. 75, no. 2, pp. 436-480, 1997.

[9] T. Strohmer and R. Heath, “Grassmanian frames with applications to coding and communication,” *Appl. Comput. Harmon. Anal.,* vol. 14, no. 3, pp. 257-275, May 2003.

[10] N. Ailon and E. Liberty, “Fast dimension reduction using Rademacher series on dual BCH codes,” *Annual ACM-SIAM Symposium on Discrete Algorithms (SODA)*, San Francisco, California, USA, January 20-22, 2008.

[11] S. Howard, R. Calderbank, and S. Searle, “A fast reconstruction algorithm for deterministic compressive sensing using second order Reed-Muller codes,” *Conference on Information Systems and Sciences (CISS)*, Princeton, NJ, Mar. 2008.

[12] N. Y. Yu, K. Feng, and A. Zhang, “A new class of near-optimal partial Fourier codebooks from an almost difference set,” *Des. Codes Cryptogr*. Sep. 2012.

[13] S. Gurevich, R. Hadani, and N. Sochen, “On some determistic dictionaries supporting sparsity,” *J. Fourier Anal. Appl*., vol. 14, no. 5-6, pp. 859-876, 2008.

[14] Z. Xu, “Deterministic sampling of sparse trigonometric polynomials,” *Journal of Complexity*, vol. 27, pp. 133-140, 2011.

[15] N. Y. Yu, “Deterministic compressed sensing matrices from multiplicative character sequences,” *45th Annual Conf. Information Sciences and Systems (CISS)*, Johns Hopkins University, Baltimore, MD, Mar. 2011.

[16] N. Y. Yu, “Additive character sequences with small alphabets for compressed sensing matrices,” *IEEE International Conference on Acoustics, Speech and*

Signal Processing (ICASSP), Prague, Czech Republic, May 2011.

[17] S. Li, F. Gao, G. Ge, and S. Zhang, "Deterministic construction of compressed sensing matrices via algebraic curves," *IEEE Trans. Inf. Theory*, vol. 58, no. 8, pp. 5035-5041, Aug. 2012.

[18] N. Y. Yu, "On statistical restricted isometry property of a new class of deterministic partial Fourier compressed sensing matrices," *ISITA* 2012, pp.287-29, Honolulu, HI, Oct. 2012.

[19] A. Amini, V. Montazerhodjat, and F. Marvasti, "Matrices with small coherence using *p*-ary block codes," *IEEE Trans. Sig. Proc.*, vol. 60, no. 1, pp. 172-181, Jan. 2012.

[20] N. Y. Yu and Y. Li, "Deterministic compressed sensing with a new class of partial Fourier matrices," submitted in *IEEE Trans. Inform. Theory,* Nov.2012

[21] D. Needell and J. A. Tropp, "CoSaMP: Iterative signal recovery from incomplete and inaccurate samples," *Appl. Comput. Harmon. Anal.*, vol. 26, pp. 301-321, 2009.

[22] M. Fornasier and H. Rauhut, "Compressive sampling." Chapter in Part 2 of *the Handbook of Mathematical Methods in Imaging* (O. Scherzer Ed.), Springer, 2011.

[23] M. Davenport, M. Duarte, Y. Eldar, and G. Kutyniok, "Introduction to Compressed Sesning," Chapter in *Compressed Sensing: Theory and Applications*, Cambridge University Press, 2012.

[24] M. Stéphane "A Wavelet tour to signal processing." *3rd edition, The Sparse Way,*

Oct.9, 2008.

[25] K. Brandenburg, “MP3 and AAC explained,” in *AES 17th International Conference on High-Quality Audio Coding*, Sep. 1999.

[26] W. Pennebaker and J. Mitchell, “JPEG: Still image data compression standard,” Van Nostrand Reinhold, 1993.

[27] D. S. Taubman and M. W. Marcellin, “JPEG 2000: Image Compression Fundamentals, Standards and Practice,” *Kluwer*, 2001.

[28] L. M. “Compressive sensing MRI.” *IEEE Signal Processing Magazine*. vol. 25, no. 2, pp.72-82, Mar. 2008.

[29] J. Y. Choi, M. W. Kim, W. Seong, J. C. Ye, “Compressed sensing metal artifact removal in dental CT.” *Proc. IEEE International Symposium on Biomedical Imaging (ISBI)*, pp. 334-337, June 28–July 1, 2009, Boston, USA

[30] Richard Baraniuk, “Compressive sensing,” *IEEE Trans. Signal Processing Magazine*, 24(4), pp. 118-121, July 2007.

[31] J. Kang, H. Lee, K. Kim, “Detection-directed sparse estimation using Bayesian hypothesis test and belief propagation.” submitted on *IEEE Trans. Signal Processing*, Nov. 2012.

[32] Haar, A., “Zur Theorie der orthogonalen Funktionensysteme,” (*Erste Mitteilung*), Math. Ann. 69. 1910.

[33] A. Bhardwaj and R. Ali, “Image compression using modified fast haar wavelet transform.” *World App. Sci. Jor*. 7(5), 647–653, 2009.

[34] E. Candès and M. Wakin, “An introduction to compressive sampling.” *IEEE*

Signal Processing Magazine, 25(2), pp. 21 - 30, March 2008.

[35] G. Kutyniok, "Compressed Sensing: Theory and Applications." *Preprint*, March 12, 2012.

[36] M. Rudelson and R. Vershynin, "On sparse reconstruction from fourier and gaussian measurements," *Communications on Pure and Applied Mathematics*, vol. 61, pp. 1025–1045, 2008.

[37] W. Xu and B. Hassibi, "Efficient compressive sensing with determinstic guarantees using expander graphs." *IEEE Information Theory Workshop*, Lake Tahoe, September 2007.

[38] N. Y. Yu, "New construction of a near-optimal partial Fourier codebook using the structure of binary m-sequences," *IEEE International Symposium on Information Theory (ISIT)*, pp. 2446-2450, Cambridge, MA, July 2012.

[39] D. L. Donoho and M. Elad, "Optimally sparse representation in general (nonorthogonal) dictinaries via l1 minimization," *Proc. Natl. Acad. Sci.*, vol. 100, pp. 2197-2202, Mar. 2003.

[40] L. R. Welch, "Lower bounds on the maximum cross correlation of signals," *IEEE Trans. Inf. Theory*, vol. IT-20, no. 3, pp. 397-399, May 1974.

[41] J. Kovaˇcevi´c and A. Chebira, *An Introduction to Frames*, *Foundations and Trends in Signal Processing*, vol. 2, no. 1, 2008.

[42] D. Baron, M. F. Duarte, S. Sarvotham, M. B. Wakin, and R. G. Baraniuk, "An information-theoretic approach to distributed compressed sensing," in *Proceedings of the 43rd Allerton Conference on Communications, Control, and*

Computing, Sep. 2005.

[43] K. Ni, P. Mahanti, S. Datta, S. Roudenko, D. Cochran, "Stability of efficient deterministic compressed sensing for images with chirps and Reed-Muller sequences," *Proc. SPIE* 7497, MIPPR 2009: Medical Imaging, Parallel Processing of Images, and Optimization Techniques, 74971S, Oct 30, 2009.

[44] J. A. Tropp and A. C. Gilbert., "Signal recovery from random measurements via orthogonal matching pursuit," *IEEE Trans. Inf. Theory*, vol. 53, no. 12, pp. 4655-4666, 2007.

[45] F. J. MacWillams and N. J. A. Sloane, *The Theory of Error Correcting Codes*, Amsterdam, The Netherlands: North Holland, 1986.

[46] H. Rauhut. "On the impossibility of uniform sparse reconstruction using greedy methods." To appear, *Sampl. Theory Signal Image Process.*, 2008.